LIFE PROJECT

"Participatory and multi-level governance process to design a transformational climate change adaptation project at Cala Millor beach from an integrated and multidisciplinary science-based approach".

DELIVERABLE NUMBER

3.3: Report on exposed elements and historical impacts in Cala Millor.

PROJECT ACRONYM	**LIFE AdaptCalaMillor**
GRANT AGREEMENT NUMBER	**LIFE21/GIC/ES/101074227**
CALL AND TOPIC	**LIFE-2021-SAP-CLIMA-GOV**
FUNDING BODY	**CINEA**
PROJECT DATES	**1st of January 2021 – 30th of April 2027**
COORDINATOR BENEFICIARY	**Directorate General of Energy and Climate Change (DGECC)**
WEBSITE	

DELIVERABLE NUMBER	D3.3
DELIVERABLE TITLE	***Report on exposed elements and historical impacts in Cala Millor***
WORK PACKAGE AND TASK NUMBER	WP3; Task T3.2.
LEAD PARTICIPANT PARTNER	UIB and IMEDEA-CSIC
DISSEMINATION LEVEL	**public**
DELIVERY DUE DATE	31/03/2024
LAST MODIFIED DATE	31/03/2024
AUTHORS (alphabetical order)	Lluís Gómez-Pujol, Marta Marcos, Maria Mulet
CONTRIBUTORS (alphabetical order)	Àngels Fernàndez-Mora, Alejandro Orfila, Elena Sánchez-García.

This project has received funding from the European Union's LIFE programme under grant agreement Nº LIFE21/GIC/ES/101074227

Disclaimer:The information and views set out in this report are those of the author(s) and do not necessarily reflect the official opinion of the European Union. Neither the European Union institutions and bodies nor any person acting on their behalf may be held responsible for the use which may be made of the information contained therein.

Project partners:

Cita: Gómez-Pujol, L., Marcos, M., Mulet, M. (2024). DELIVERABLE NUMBER 3.3: Report on exposed elements and historical impacts in Cala Millor. http://doi.org/10.25704/Z7P4-8221

EXECUTIVE SUMMARY

In this report we provide a comprehensive description of the upper beach as an exposed element in front of wave climate at Cala Millor beach, including its mean and extreme regimes, using all available in-situ and modeled data. Our main focus is on extreme wave events, and on the quantification of the impact of these episodes on the beach response, in terms of erosion patterns measured as changes in the shoreline position. We also characterize the regional synoptic patterns that generate the different types of wave extremes observed in the beach. Cala Millor has been extensively monitored since 2011, making this spot one of the best monitored beaches worldwide. Additionally, we have used numerical model outputs that have been recently generated with a coupled hydrodynamic-wave model covering all the Mediterranean basin with unprecedented spatial resolution, reaching 200 m in coastal regions. The modeled data set spans the period 1950-2022, allowing to extend the observational period several decades. The model has been forced with surface mean sea level pressure and wind fields from the state-of-the-art ERA5 atmospheric reanalysis, and these data have also been used to describe the atmospheric conditions over the western Mediterranean basin during extreme episodes.

In order to use the extended model period to describe the wave climate and the associated synoptic patterns, we have evaluated the consistency between in-situ and modeled waves datasets for their overlapping period. We found that for significant wave height, Hs, both data sets are highly consistent and correlated, although we also find that the model time series underestimates extreme values in the observations. This is a general shortcoming of modeled data, partly due to the relatively low resolution of the atmospheric forcing of the model, that is only 0.25° in latitude and longitude. Also, despite the high spatial resolution of the regional model, it is not expected to accurately reproduce all small-scale coastal processes taking place locally in a beach. Peak period (Tp) and peak wave direction (Dp) have ranges of values that are in agreement with those observed. The comparison for the case of Dp is hampered by the limited spectral resolution of the model, which is only 15°. Despite these differences we consider that the performance of the model is good enough as to complement in-situ observations. Also, the larger spatial scale makes it suitable to investigate regional patterns that are associated with the local wave climate in Cala Millor. The use of numerical wave simulations to investigate wave climate characteristics and changes, despite generally suffering the same shortcomings as the ones pointed out above, is common practice.

Since we focus on extreme wave events that have had a plausible effect on the beach state and damage, our definition of extremes encompasses both the value of wave height (Hs) and its duration. Namely, extreme events have been defined as those exceeding 1.5 m in Hs during at least 6 h. This resulted in 79 events in the observational record and 688 in the modeled time series. In observations, maximum Hs is 5.45 m, and the range of duration is from 6 to 380 hours. The maximum Hs in modeled data are clearly lower (4.68 m), which is reflected in the return level curves. The regional numerical simulation has been extensively validated in the entire Mediterranean basin and has shown a very good performance when compared to both in-situ and satellite-based Hs measurements. However, these datasets correspond to deep water

environments. Small scale processes, linked to wave shoaling and in response to small bathymetric features are not expected to be accounted for. We recall that the model resolution is of the order of 100 m along the coast; this is an exceptionally high resolution for a regional domain, although it is not intended to simulate small scale coastal processes. The underestimation of return levels obtained with regional modeled data with respect to in-situ observations is a proof of the relevance of these measurements and advocates for the need of continuous nearshore processes monitoring.

The regional model is suitable to provide basin-scale information in relation to identified extreme events in Cala Millor beach. We aimed at describing the synoptic patterns that are responsible for these local extreme episodes. Given the large number of events, we have applied techniques for reducing the dimensionality and that allow the identification of regional patterns in the atmospheric and oceanic conditions during extreme events. The two techniques applied here are EOF (Empirical Orthogonal Function) decomposition and K-means clustering. Both are very different to each other but provide consistent results, thus increasing the robustness of the conclusions. We have identified the dominant atmosphere-ocean patterns that generate wave extremes in Cala Millor: northerly winds from the Gulf of Lions over the central part of the basin, easterlies from the Tyrrhenian Sea and perturbations generated within the cyclogenesis area of the Gulf of Genoa. These patterns appear more clearly in the K-means classification than in the EOF decomposition.

Finally, we have tried to link the occurrence of extreme episodes with changes in the state of the beach. To do so, we have explored the observations of the beach shoreline position that were coincident with the episodes that we have identified. Because of the relatively coarse temporal sampling of the shoreline position, the occurrence of an event and its corresponding shoreline measurements are often a few days apart. This exercise is complex for various reasons. First, there are only a few locations for which long-term nearshore wave observations and shoreline positions are available worldwide. Secondly, there is no unequivocal response from the beach. Rather, it depends both on the forcing and on its initial state. This means that if the beach is recovering (accreting) from a storm, it may be more sensitive to the effect of a new storm. In other words, extreme events are related to shoreline changes when 1) the event is energetic enough to cause beach erosion or 2) it is subject to the forcing of a group of storms. Thirdly, we do not have continuous measurements of shoreline that provide the immediate response of the beach to every forcing event. Finally, we oversee other factors that may be relevant, like the changes in mean sea level that alter the baseline level upon which the storm waves reach the coastline. Interannual variability in mean sea level is of the order of a few tens of cm (at most) in the Mediterranean Sea. In any case, the results of the analyses show that in most of the storms analyzed for the studied period, some of which with long-range return periods, no damage is caused beyond the dry beach. The largest storms, as verified from coastal video monitoring images, involve a loss and/or redistribution of sediment, damage to beach furniture and occasionally transportation of sand to the promenade. The risk study based on press reports associated with the storm dates has not produced results that show either flooding or losses to infrastructure or private properties in Cala Millor.

INDEX

1. INTRODUCTION

This document collects the results of the historical impacts report and the elements exhibited in Cala Millor, with the ultimate objective of assessing the vulnerability and exposure of natural and socioeconomic assets of Cala Millor within the framework of the LIFE AdaptCalaMillor project.

From an operational point of view, the results of this report will serve to establish the typology of extreme events to associate with scenarios of sea level rise due to climate change and, based on them, model the impact on the natural and socioeconomic assets of the area.

In doing so, the concept of risk, following the footsteps of the different reports of the Intergovernmental Panel on Climate Change (IPCC), is understood as the probability that an adverse event of natural origin and its consequences will occur in a given period of time. Therefore, the risk derives from a combination of threats and the vulnerability of the exposed elements that will result in a potential for severe disruption of the affected society or element once the adverse event has materialized.

We understand risk as the potential event of natural origin that acts as an external risk factor on a natural and/or anthropic system in a specific place and with a determined intensity and duration. In the case at hand, marine storms or groups of storms and their effects on the beach.

1.1 Extreme events and beach erosion

The main cause of recurring morphological variability and shoreline change on the coast, from weeks to years and sometimes decades, is coastal storms, during which beaches and dunes suffer erosion (Castelle and Harley, 2020). Although in embayed and sheltered beaches, alongshore transport can control signals of coastal change in the form of beach rotation; on most open coasts, storm-induced beach erosion involves the cross-shore transport of sediment. During storms, sediment from the beach, and sometimes from nearby dunes, is carried seaward by undertow flow, and during post-storm conditions, wave nonlinearities slowly push back the sediments from the upper shoreface to the subaerial beach (Hoefel and Elgar, 2003).

A single isolated coastal storm can have a dramatic and long-lasting impact on the coast (Harley et al., 2017), but the combined impacts of a series of less severe storms can also cause severe coastal erosion (Morales-Márquez et al., 2018). Coastal storm events occur in rapid succession separated by short time intervals, 2 to 3 days, and tend to be called storm clusters or storm groups. They can have a significant impact on the coasts on the basis of the wave height and peak period, but if because storm cluster duration they coincide with other hazards, such as spring high tide or storm surge, then the synchronicity of the environmental parameters can enhance the coastal erosion hazard (Guisado-Pintado and Jackson, 2018).

In coastal sciences there is no univocal way to decide what defines an extreme event, and concepts such as storm or **extreme storm** are used without semantic difference. Storm events can be characterized by variables such as storm magnitudes (wave height), storm direction, tidal excursion or water level surge for a time period (Guisado-Pintado and Jackson, 2018). Other approaches also consider storm impacts (i.e. dune erosion or coastal flooding) that transites from

the distinction between extreme event and extreme impact (McPhillips et al., 2018). Nevertheless the definition of wave extreme event or coastal storm are based on meteorological and oceanographic forcing variables. According to Castelle and Harley (2020) and referred to wave-dominated coasts, a storm is defined as an event in which wave height exceeds a certain threshold. Such thresholds very often are proposed subjectively on the basis of typical erosion features observed along the coast of interest, even though more objective and transferable threshold determination is the use of probability distribution of the **wave height** (Harley, 2017). For example the 0.5% exceedance level of the 5% exceedance level (e.g. Cañellas et al., 2007; Castelle et al., 2015). Duration is another critical parameter in characterizing wave storms. **Storm duration** can therefore be described as the duration over which wave height exceeds the threshold considered. Additionally duration can be also defined as the time when wave height exceeds another probability distribution quantile (e.g. the 25% exceedance level) (Masselink et al, 2014). There is a wide range of meteorological criterions to restrict the **time-lapse between individual storm events** and unravel if they are part of the same storm (Harley, 2017). These criterions can range from 30 hours to 2 weeks, but there are some examples that attend 39 ways. The wide range of criterions can produce important differences in the number and duration of defined storm events (Sénéchal et al., 2017). In any case, storm wave conditions can coincide with spring high tides, storm surge or changes in differing offshore wave directions that result in an increase in the coastal hazard. Therefore water levels, such as the **tide level**, the empirical vertical **wave run-up** and **storm surge** estimation should be summed to wave effects (Young et al., 2016).

Beach erosion is understood as the **net loss of beach sediments** over a cross-shore 2D section of the beach profiles referred to a timescale of interest. This phenomenon is manifested in a different number of morphological evidences on the coast, including a reduction on subaerial beach area, shoreline landward migration, sediment loss out of the system, lowering of the subaerial beach profile, the presence of beach scarps and undermining of dunes, cliffs and back beach infrastructure. Beach erosion is one of the most common impacts of extreme events. In most cases storm events cause a simple redistribution of beach sediment, such that subaerial beach loss sediments toward the surf zones (Álvarez-Ellacuría et al., 2011; Gómez-Pujol et al. 2011); but for a particular extreme event this loss of sediment might extend from shallow waters to depth of closure. This immense loss of sediment can take decades for the beach to recover from (Morales-Márquez et al., 2018). The magnitude of subaerial beach volume change caused by a storm or by a storm cluster is an important variable in coastal management as it helps to design the determination of appropriate setback lines (Callaghan et al., 2009). In doing so it is assumed that a storm or cluster storm event with a given return period (e.g. annual to 100 years return period event) will result in an equivalent loss in subaerial beach volume. This volume of sediment is known as **storm demand**, and once it is estimated, a proper buffer distance separating exposed elements from the shoreline should be implemented (Kinsela et al., 2017).

1.2 Historical impacts and exposed elements

Coastal storms, due to their harmful potential, with processes such as the erosion of beaches and dunes, overwashing and beach flooding, are understood as **coastal hazards** (Jiménez et al., 2012; Luque et al., 2021). Coastal hazards become coastal damages when there is an overlap between the area of influence of storm-induced processes and the area of human intensive use (i.e. leisure, residential and infrastructure development) or when other natural systems can be

seriously affected (Toimil et al., 2017). Most often, the energy content of storms is understood as an indicator of the damage induced on the coast. Greater damage should be associated with the impact of a greater number of storms. However, this is not necessarily true because other parameters can modulate the morphodynamic response and induced coastal hazard and therefore storm time series are not sufficient to reconstruct the temporal evolution of damage along a coastal zone (Jiménez et al., 2012). Cooper et al. (2004), addressing the impact of storms along the west coast of Ireland, concluded that reconstructing storm impacts using damage records is difficult because these data sources are scarce and difficult to attribute to specific storms. In other words, one of the main difficulties in reconstructing the **time history of storm effects** is finding reliable and comprehensive long-term data on coastal response. This difficulty can be extended to collecting the damage caused by storms, differentiating the type of damage and its cost. A growing approach in risk studies is the use of **newspapers** and local library archives among other **regional historical data sources** in order to identify noticeable hazardous events (Ibsen and Brundsen, 1996). Jiménez et al. (2012) and Sancho-García et al. (2021) have demonstrated the ability of press news to be used as proxy indicators of the impact of storms and the damage caused, although with several biases and uncertainties.

Within this context, the main goal of this report is to analyze the temporal extent of sea storms and storm groups at Cala Millor and the associated coastal damage on the natural and human systems. In doing so, we will start from wave data measured in situ, and from modeling and we will focus on the loss of the subaerial beach surface, since there is a series of data from the SOCIB beach monitoring infrastructure from 2011 to 2022, as well as in the exploration of different records, including the local press, to detect which elements of natural and anthropic systems are exposed to coastal damage.

2. STUDY SITE

Cala Millor (CLM) beach is located on the north-eastern coast of Mallorca in the Western Mediterranean Sea (Fig. 2.1). It is a carbonate sandy beach, ~2 km in length, with a concave shape fronted by a boulevard wall over which hotels and residential houses span over a Holocene dune system and the remnants of a man-filled humid zone (Tintoré et al., 2009). CLM is an intermediate beach with a configuration of transverse and crescentic bars20 which means that there is a large alongshore shoreline variability and also rip channels (Gómez-Pujol et al., 2011; Álvarez-Ellacuría et al., 2011).

The beach bottom is characterized by the cropping out of rock reefs, and at depths from 6 to 35 m there are paleochannels and the seagrass meadow of the endemic *Posidonia oceanica*, which acts as a cover to sediment exchange and a friction obstacle to waves (Infantes et al., 2009). The beach sediments at CLM consist of medium carbonate bioclastic marine sands with a median diameter of approximately 1.8 phi. These sediments correspond to a mid-Holocene attached regressive barrier that prograded landward through a foredune and a field of parabolic dunes (Gómez-Pujol, 2014).

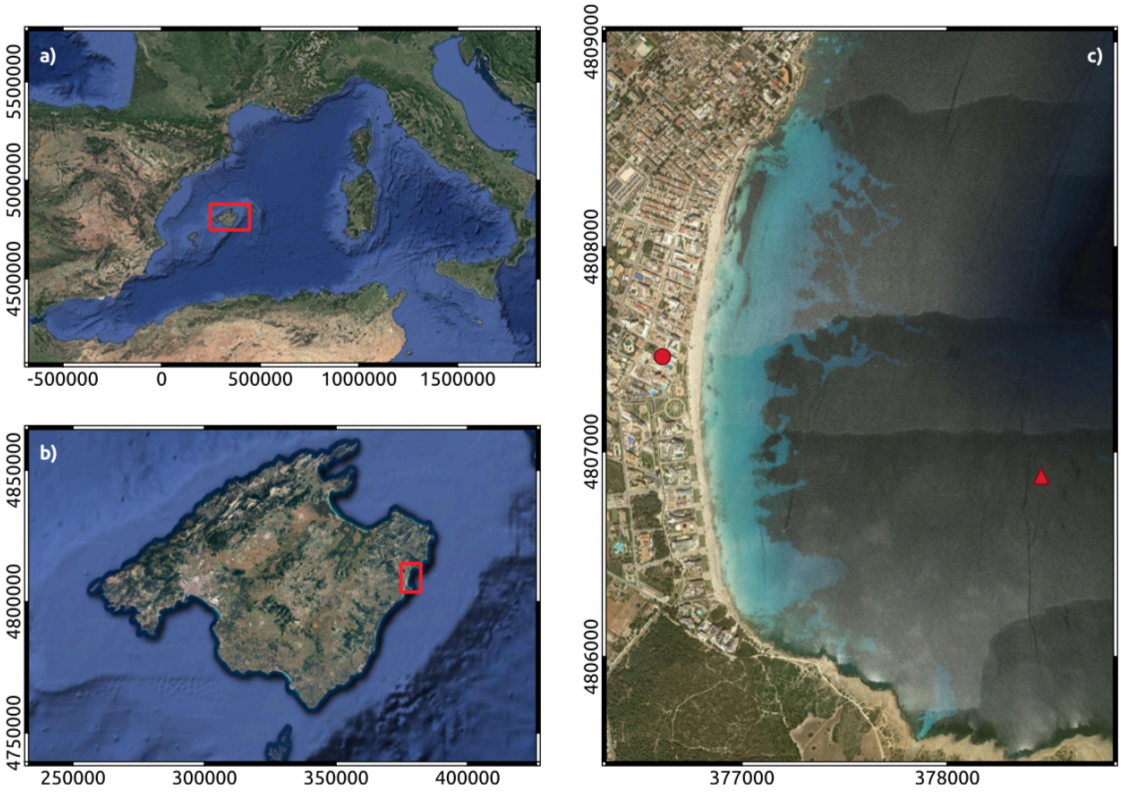

Fig. 2.1. (**a**) Western Mediterranean Sea. Red box indicates the location of Mallorca. (**b**) Mallorca. Red box indicates the location of Cala Millor Beach (CLM). (**c**) Cala Millor beach (CLM). The red dot indicates the location of the video-monitoring station and the red triangle the location of the submerged ADCP.

CLM is exposed to mild-moderate wave conditions, with a mean significant wave height Hs = 0.52 m and peak period Tp = 6.1 s. The wave climate is strongly seasonal dominated, characterized by low and short mostly locally-formed waves due to summer sea breezes, and higher and longer well-developed waves during winter that can reach 4 m in height (Morales-Márquez et al., 2018). Tides are negligible, since the daily tidal range is ~0.2 m. Surge components induced by wind or atmospheric pressure can increase the sea level by up to 1 m (Orfila et al., 2005). However, there is an inter-annual sea-level variation up to 0.5 m due to inter-annual fluctuations of sea-temperature, internal oscil- lations in the Mediterranean basin, and the interaction of internal currents in the Western Mediterranean sea (Marcos et al., 2008; Calafat and Gomis, 2009).

3. MATERIALS

This section describes the data used throughout the document, including measurements and outputs of numerical simulations.

3.1 Coastal observations

We use in-situ measurements from SOCIB's Modular Beach Integral Monitoring System (MOBIMS) located at CLM beach (Mallorca), described and published in Fernández-Mora et al. (2023). The system consists of a SIRENA video monitoring station, a Nortek AWAC instrument, a Vaisala

WXT520 weather station and 6-month beach and sediment surveys. The main objective of these platforms, that have been working since 2011, is to provide continuous measures on beach shoreline and sediment budget evolution, along with the factors influencing them. This includes both the oceanic and the atmospheric data.

SIRENA makes extracting the shoreline position possible during daylight time. The Vaisala WXT520 measures barometric pressure, air temperature, wind velocity and direction, relative humidity and precipitation. The Nortek AWAC measures current velocity, direction profile and wave height, period and direction; it is a self-contained instrument and data is recovered every 6 months.

Throughout this project, the data resulting from SIRENA (periodic shorelines) and the Nortek AWAC are used. Below, a comprehensive description of this equipment and used variables is presented.

3.1.1. Waves observations

The dataset spans from 2011/05/20 up to 2023/10/25, with a gap from 2019/05/20 to 2019/10/29 due to an instrument failure, with hourly frequency. The variables considered are included and briefly described in Table 3.1.

Table 3.1. Summary of the AWAC observed variables.

Variable	Description	Units
aw_lat	Latitude coordinate at which the instrument is located	degrees
ar_lon	Longitude coordinate at which the instruments is located	degrees
w_depth	Depth of the instrument	m
aw_time	Timestamp of each observation value	–
aw_Hs	Sea surface wave significant height	m
aw_tp	Sea surface wave peak period	s
aw_Dp	Sea surface wave peak direction	degrees
aw_Ec	Error code	–

3.1.2. Shoreline position

The shoreline data comprises a georeferenced set of waterline positions, obtained auto-matically and supervised manually from georeferenced plan-view images. The earliest record is from 10th of June of 2011 and the last one corresponds to 23rd of December of 2022, with a temporal frequency of approximately two weeks between measurements (Figure 3.1). The data set was published in 2023 (Fernández-Mora et al., 2023).

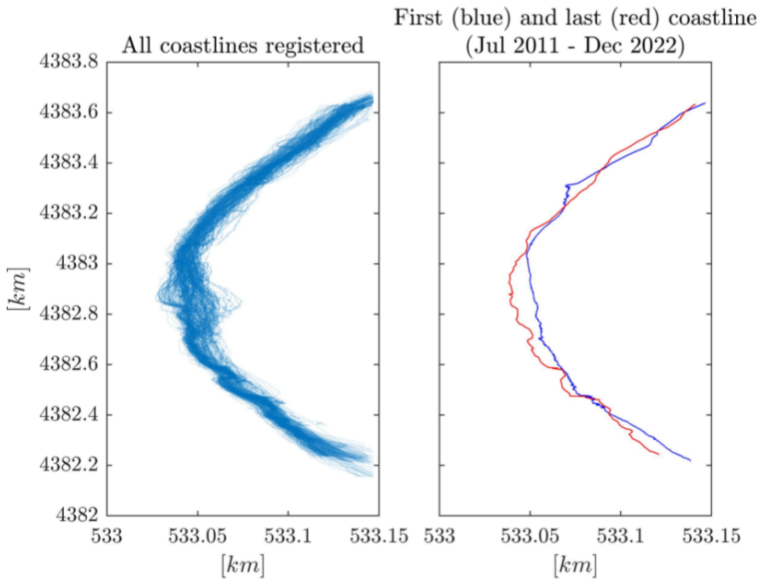

Fig. 3.1. Overview of CLM shoreline variability. On the left, overlap of all registered shorelines. On the right, first and last observed shorelines.

The SIRENA system, developed and installed by IMEDEA (Nieto et al., 2010), allows extracting near-shore data, including shoreline position among other parameters (Stockdon and Holamn, 2000; Lippmann and Holman, 1989). The system consists of five cameras situated at coordinates 39º59'N and 3º38'E, 46.6 m above sea level. Operating hourly during daylight time, SIRENA captures 4500 images during the first 10 minutes every hour (Nieto et al., 2010). These images are used to create various statistical outputs, including snapshots, mean time exposures, time variance, and time stack images. Through photogrammetric techniques, the images are georectified and the shoreline is obtained (Fernández-Mora et al., 2023).

3.2 Numerical simulations of wave data

The simulated wave data have been generated by the ocean numerical model SCHISM (Semi-implicit Cross-scale Hydroscience Integrated System Model), implemented as described in (Toomey et al., 2022). SCHISM (Zhang et al., 2016) is a model with a main hydrodynamic module that runs on a 2D unstructured (i.e., irregular) mesh and that has been applied in this work over the entire Mediterranean Sea. The hydrodynamic module can be coupled to other modules to represent marine processes, such as waves or sediment transport. In this work, the model has been run coupled with the wave module (Wind Wave model, WWM).

The model outputs provide hourly sea level and wave data at every grid point in the Mediterranean basin, with a spatial resolution that varies between 20 km in the open sea down to 200 m along the coastlines, during the period 1950-2021, spanning a total of 72 years. The model has been run with a spectral resolution of 15º. The bathymetry used in the model is EMODnet (European Marine Observation and Data Network), using data from 2018, which has a nominal resolution of approximately 115x115 m. Overall, the unstructured mesh covering the Mediterranean basin is composed of 379,762 nodes. The density of points is higher along the coast to account for changes in waves due to shoaling processes, and thus the morphology needs

to be accurately determined. For these points, the coordinates and the depth of the seafloor are prescribed. The depth has been interpolated to the desired mesh points from the bathymetry.

The variables provided by the model and considered in each node are listed in Table 3.1. All variables were validated by comparing model outputs to observations from tide gauges and buoys in the Mediterranean basin (Toomey et al., 2022). The results of the validation showed an excellent agreement between the model-generated data and the observations for all the variables. In particular, significant wave heights displayed correlations with a median value of 0.92, the mean square error median of 21.6 cm, and mean square error in extreme events median of 41.9 cm, using all in-situ buoy data available.

Table 3.1. Summary of the hindcast variables.

Variable	Description	Units
hi_lat	Latitude coordinate at which the instrument is located	degrees
hi_lon	Longitude coordinate at which the instruments is located	degrees
hi_depth	Depth of the instrument	m
hi_time	Timestamp of each observation value	–
hi_Hs	Sea surface wave significant height	m
hi_tp	Sea surface wave peak period	s
hi_Dp	Sea surface wave peak direction	degrees

Two sets of data are obtained with this model. Both of them span the period from 1st of January of 1950 to 31st of December of 2020. The first set consists of an irregular mesh of 132 nodes close to CLM, used to detect extreme events during the entire period. Figure 3.2 illustrates the regional domain and CLM location, as well as the irregular mesh mentioned earlier. The node number 102 of the mesh (not shown in the figure for the sake of clarity) is the closest to the location of the AWAC instrument, used in the project to compare results between observations and model.

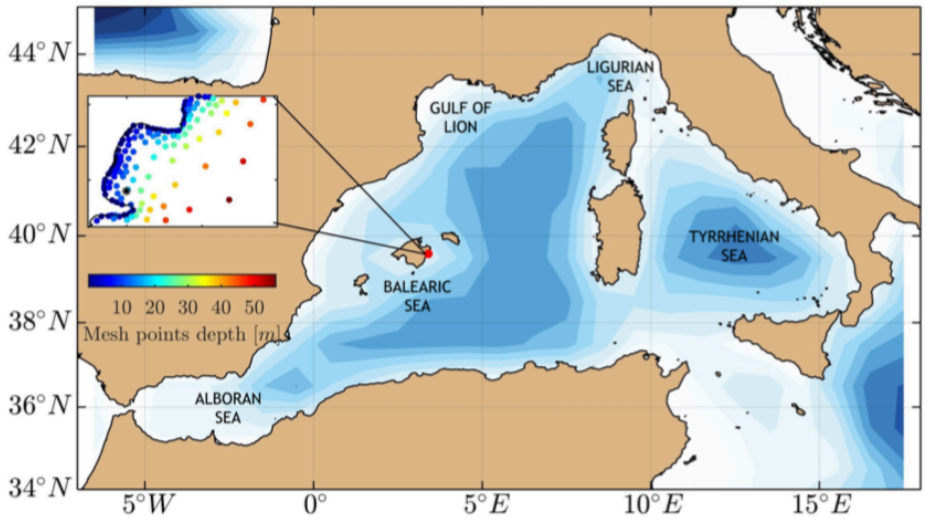

Fig. 3.2. The Mediterranean region considered throughout this document, with a closer look at CLM beach, where the AWAC instrument is located.

The second set provides data on a regional scale, over the western Mediterranean basin. The nodes of the model considered are only the ones with depth greater than 50 m. The data of the irregular mesh shown in Figure 3.3a have been linearly interpolated onto a regular grid with 0.1 deg spatial resolution (Fig. 3.3b).

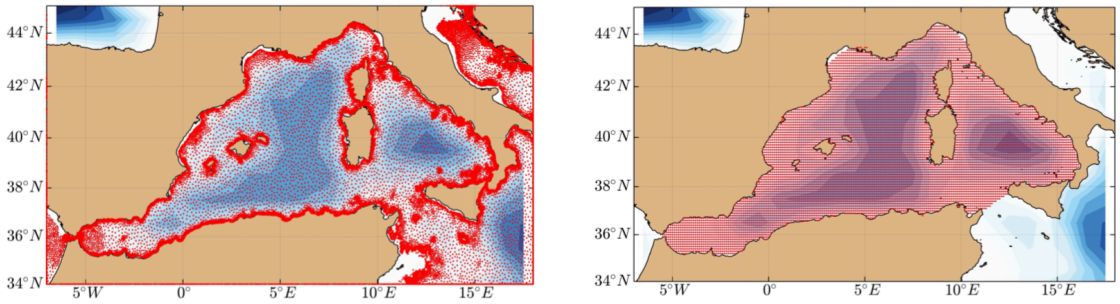

Fig. 3.3. Regional domain. (a, left panel) In red, coordinates where SCHISM provides wave data for the period 1950-2022. (b, right panel) coordinates at which we interpolated SCHISM wave data.

3.2 Atmospheric fields

Atmospheric mean sea level pressure and surface wind fields have been obtained from ERA5 reanalysis (Herbasch et al., 2023), at 0.25º spatial resolution and hourly temporal sampling (Fig. 3.4 and Table 3.2). These fields are used to characterize the regional synoptic patterns during and prior to defined extreme events. Moreover, this is the same set used during the forcing of SCHISM to obtain oceanic variables, thus being fully consistent with wave data.

Table 3.2. Summary of the ERA5 atmospheric variables.

Variable	Description	Units
lat	Latitude coordinate	degrees
lon	Longitude coordinate	degrees
time	Timestamp of each observation value	–
u10	Horizontal wind velocity	m/s
v10	Vertical wind velocity	m/s
mslp	Mean sea level pressure	Pa

3.3 Regional impact data sources and impact published news

To establish a record of elements damaged by the coastal storms, we have started from the archives of the two newspapers with the largest circulation in Mallorca, Última Hora (https://www.ultimahora.es/hemeroteca.html) and Diario de Mallorca (https://www.diariodemallorca.es/hemeroteca/), while at the same time the published bibliography that may include information on the matter has been reviewed.

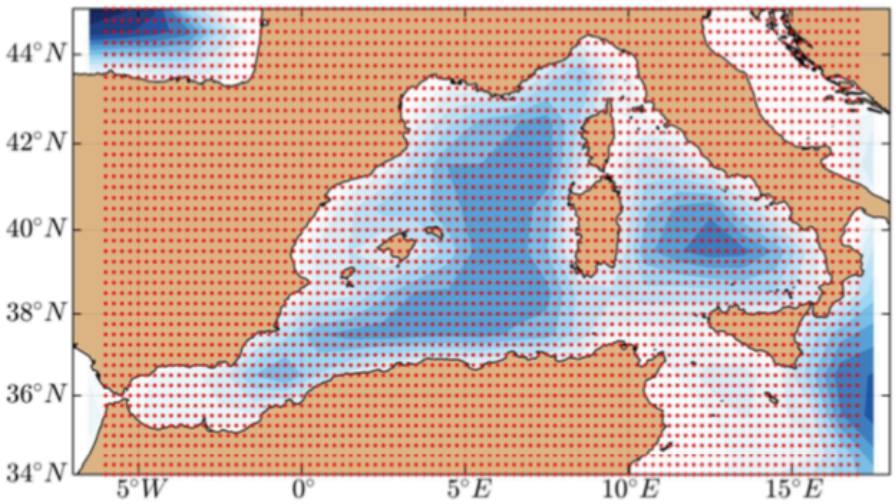

Fig. 3.4. ERA5 Coordinates at which atmospheric data have been obtained (regional domain).

4. METHODOLOGY

This section describes the approaches and methods that have been applied to pre-process and analyze the data described in the previous section.

4.1 Selection of extreme wave events at Cala Millor

Sensitivity analysis plays a crucial role in determining thresholds for defining extreme events, such as storms. In this context, sensitivity analysis involves systematically testing different threshold values to understand their impact on event detection and to strike a balance between capturing a sufficient number of events and ensuring their significance in terms of intensity.

Following the standard Peak over Threshold procedure (Coles, 2001), our study defines an extreme event as a period lasting at least six consecutive hours with a Hs exceeding 1.5 meters. Additionally, to distinguish independent events, a minimum separation of 48 hours is required.

This temporal criterion aims to prevent the artificial splitting of events into multiple occurrences. Through our analysis, we have explored variations in these thresholds to refine our definition of extreme events. Various threshold combinations were evaluated to assess their effectiveness in capturing extreme wave events. For instance, we tested a shorter separation period of 24 hours, which, while splitting some dependent events, proved less effective in capturing the full spectrum of extreme events. Similarly, raising Hs threshold to 2 meters, while enhancing the intensity criterion, led to the exclusion of certain events, potentially resulting in an incomplete representation of extreme conditions.

Our final threshold selection involves a trade-off between the number of detected events and their intensity. This iterative process resulted in the identification of 79 independent extreme wave events within the observational data spanning from 2011 to 2022. Independent events require a separation of at least 48 h. This ensures that one event is not artificially separated into

two. Other thresholds have been tested: a separation between events greater than 72 h merges independent events; significant wave height greater than 2 m misses some events.

In comparison, a broader timeframe encompassing modeled data from 1950 to 2020 revealed 688 extreme wave events.

It is worth noting that the sensitivity analysis was conducted exclusively on observational data. The results indicated varying event counts based on different threshold configurations (Table 4.1):

- For a minimum wave height of 1.5 m and a separation between events exceeding 24 h, 83 events were detected.
- With a minimum wave height of 1.5 m and a separation exceeding 48 h, 79 events were detected.
- Increasing the minimum wave height to 2 m while maintaining a separation exceeding 24 h led to the detection of 27 events.
- Similarly, for a minimum wave height of 2 m and a separation exceeding 48 h, 26 events were detected.

Table 4.1. Number of sea storm extreme events according to different criterions.

Time lapse between events	Hs min = 2 m	Hs min = 1.5 m
24 h	27	83
48 h	26	79

Thus, the final choice is a trade-off between number of events and intensity, resulting in 79 independent extreme wave events detected in the observed data (2011-2022) and 688 extreme wave events detected in the modeled data (1950-2020) which are characterized and analyzed in the following.

For each extreme wave event, we select the atmospheric and oceanic fields over the Western Mediterranean from the numerical simulation described above (see Section 2.2). Atmospheric fields are selected 12 h prior to the maximum significant wave height to represent the synoptic situation leading to the extreme. The atmospheric variables considered are surface wind (direction and module) and mean sea level pressure. On the other hand, the oceanic wave fields (Hs, wave peak period -Tp - and wave peak direction -Dp -) are extracted at the same time as the maximum significant wave height of each event. We have used ERA5 data for the period 1950-2021. This results in 75 events for the observational period of AWAC in situ data (i.e., skipping year 2022) and the 688 events for the modeled data set.

The following figures illustrate the synoptic situation and the oceanic characterisation of two selected events (Fig. 4.1). The rest of events are represented the same way and can be found in the Appendix.

4.2 Energy during extreme events

For every extreme episode we have calculated the wave energy at every time step of the event. We intend to compare the wave energy content of each event, rather than computing the

absolute value of the wave energy (Dean and Dalrymple, 1991). Therefore, we define this metric as:

$$energy \propto Hs^2 \cdot T_p$$

On the basis of this metric of the energy, two new variables have been considered throughout the analysis:

- Maximum Wave Energy During The Extreme Event (m^2/s), corresponding to the time step when the energy peaks. The units are thus given by the equation above $Hs^2 \cdot Tp$, where Hs is in meters and Tp in seconds.
- Accumulated wave energy during the extreme event ($m^2/s \cdot h$), corresponding to the sum of the energy for the duration of the event. The units are the same as above but now integrated over time at hourly time steps.

4.3 Computation of return periods of wave extremes

Observed and modeled data have been used to compute return periods of Hs corresponding to extreme events in CLM. For modeled data, the time series extracted and used correspond to the closest point in the mesh to the AWAC's location.

Given the time series, the extreme events have been selected following the methodology explained above. Once this has been done, the maximum Hs reached during each event will be the value used in the return period algorithm. Note that our definition of extreme events does not necessarily imply that maxima Hs converges to an extreme value distribution family, as we are focusing on events that may produce an impact (i.e., a combination of wave height and duration), rather than events with just very high Hs. Therefore, only a subset of events was used to fit extreme value distributions and compute return levels. Namely, we have selected a maximum of two events per year of data: 142 values for the modeled time series (71 × 2) and 22 for the observed record (11 × 2).

Return levels are computed fitting the empirical distribution of extreme Hs to a theoretical curve. The theoretical distribution chosen is the Generalised Pareto Distribution, used to model the excesses over a prescribed threshold, with cumulative distribution function as follows:

$$F(x;k,\sigma) = \begin{cases} 1-\left(1-\frac{kx}{\sigma}\right)^{\frac{1}{k}}; & k \neq 0 \quad \sigma \geq 0 \\ 1-exp\left(-\frac{x}{\sigma}\right); & k = 0 \quad \sigma \geq 0 \end{cases}$$

Where σ and k are scale and shape parameters respectively (Castillo and Hadi, 1997). Return levels are then computed as the inverse values when fitting this distribution to the extreme values observed.

Confidence intervals of the return level curves are computed via bootstrap. Boot-strap is a statistical procedure that consists of resampling the same set of data, excluding one or more observations randomly each time. It is frequently used to prevent overfitting in model management, and is closely related to deep learning techniques (Hetesberg, 2011; Michelucci and Venturini, 2021).

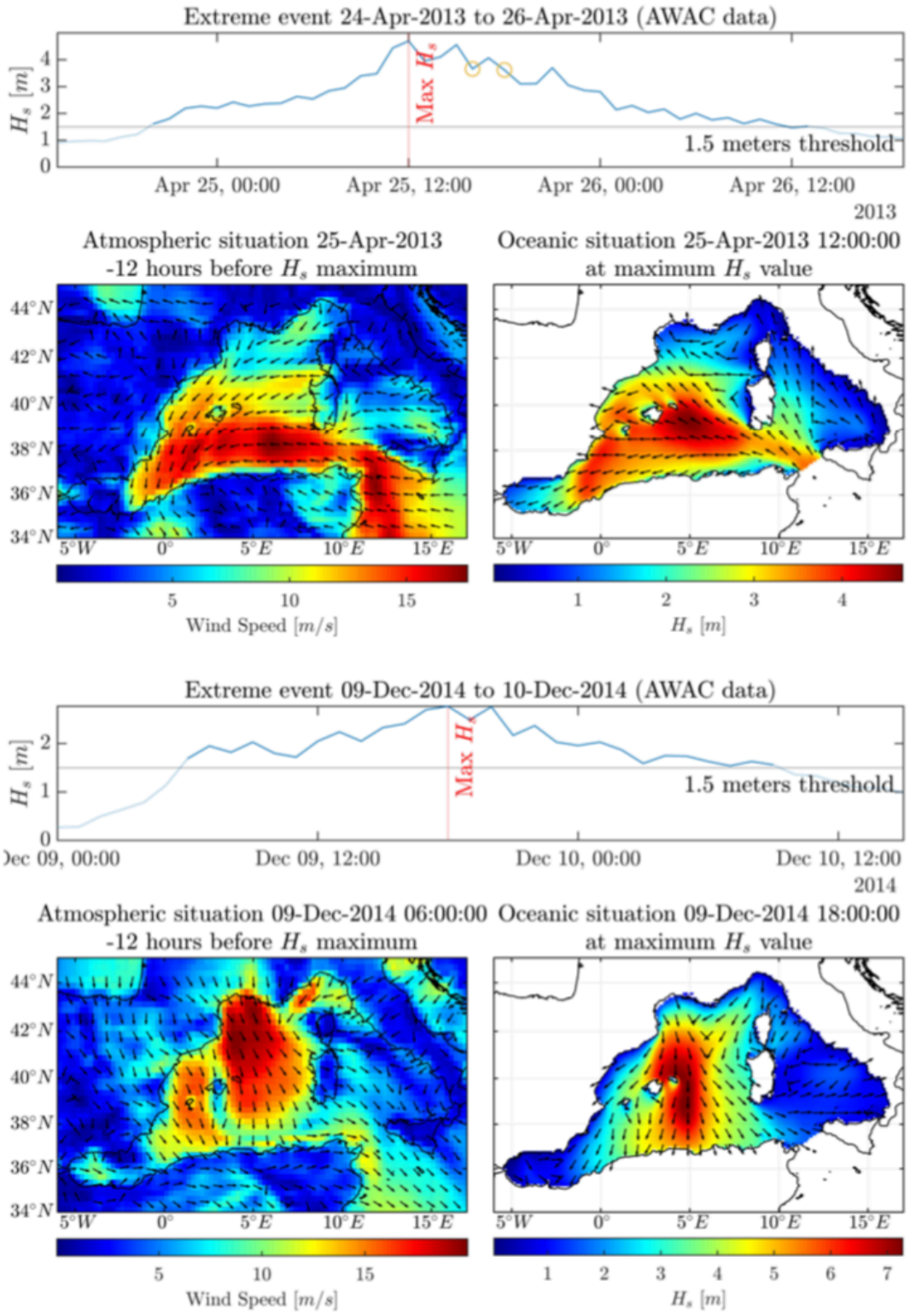

Fig. 4.1. Two of the 79 events (number 20 and 25) recorded by AWAC. On the top of the figure, Hs through the event. Darker blue represents the event period, lighter blue before and after observations but not considered an extreme event. The yellow circles indicate that the observation has an Error Code different

from 0. On the left bottom atmospheric situation. On the right bottom, the corresponding oceanic situation.

4.4 Regional clustering of extreme events

In order to reduce dimensionality of the set of data associated with the extreme events occurring at Cala Millor, regional clustering techniques have been applied to both modeled and observed data. To do so, two different techniques of clustering were used: empirical orthogonal function analysis and K-means, as described below. Both techniques were applied to significant wave height fields on the regional domain, with data on the nodes specified in Figure 3.3 for the time step coinciding with the maximum height for each extreme event. We have 688 and 75 regional Hs fields for modeled and observed extrema, respectively.

Both of these techniques consider two-dimensional sets (space × time), meaning that spatial maps of Hs are reshaped into one-dimensional vectors. This way on the first dimension we are considering the data, and on the second one the time of extreme events. From now on, we will refer to this matrix as X, with following dimensions: d_{field} rows, where every row represents a coordinate, and d_{time} columns, where every column represents the timing of an extreme event

4.4.1. Empirical orthogonal function analysis

Empirical orthogonal function analysis (or EOF from now on), also known as Principal Component Analysis (PCA), is used to identify the main patterns of variability of a spatio-temporal field (Morales-Márquez et al., 2020).

By definition, empirical orthogonal functions are eigenvalues of the covariance matrix associated to the anomaly fields of X. Given the matrix X, the first step is to subtract the temporal mean field to generate the anomalies matrix (Y). The anomaly matrix is then used to compute the covariance matrix as:

$$C = \frac{1}{d_{time}} Y Y^T$$

The next step is to diagonalize the covariance matrix, sorting the eigenvalues in descending order. The variance patterns are the eigenvectors, whereas the variance explained by each of them is given by the eigenvalues.

4.4.2. K-means clustering

The K-means algorithm finds a partition of the set of observations (considered as elements of R^{dfield}) of k clusters, where k is a prescribed parameter. This is a state-of- the-art technique that has already been applied to classify weather types at the synoptic scale (Camus et al., 2014) and spatial footprints of storminess (Enríquez et al., 2020), for example.

$$SUM = \sum_{j=1}^{k} \sum_{x_i \in C_j} ||x_i - c_j||^2$$

Given d_{time} observations, the goal is to find k elements $c_1,...,c_k \in R^{dfield}$ such that the value is minimized. We have used the implemented function *K-means*, that uses a two-phase iterative algorithm to minimize the sum of point-to-centroid distances, summed over all k clusters. In a first step, this function calculates a first guess of clustering by assigning each point to its nearest centroid. Although fast, it just provides an approximate solution. In a second step, every point is reassigned to a different cluster whenever it reduces the sum of distances within the clusters, and in doing so, every centroid is recalculated. The algorithm ensures that the solution converges to a local minimum. In order to find the global minimum, though, sensitivity tests must be carried out with different starting points.

As mentioned above, the number of clusters has to be decided beforehand. To select the optimal number of clusters we use the so-called "elbow" or "knee of a curve" as a cutoff point. This is a common heuristic in mathematical optimization to choose a point where diminishing returns are no longer worth the additional cost. This means computing the algorithm for a certain range of clusters considered, and evaluating the sum of distances from elements to centroids in each one of them, as illustrated in Figure 4.2.

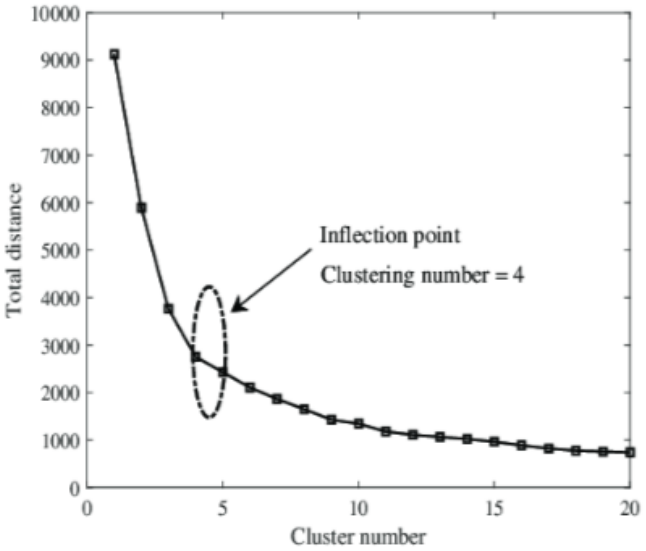

Fig. 4.2. Illustration of the "elbow" method to select the number of clusters to be prescribed in K-means algorithm.

We have used K-means clustering to provide a partition of the events based on their Hs spatial data. We are, however, also interested in the rest of variables. We have therefore calculated the atmospheric and oceanic fields associated with each cluster using the corresponding events and their classification.

4.4 Computation of the impact on shoreline position

For a given event, the alteration in the shoreline is quantified by referencing the nearest shoreline records before and after the storm. We recall that while waves time series are provided on an hourly basis, the outputs of shoreline changes are sampled fortnightly. The value of the changes

in the shoreline position from video monitoring is determined as the Root Mean Square Error (RMSE) between the two sets of data, and can be expressed as:

$$RMSE = \sqrt{\frac{1}{n}\sum_{i=1}^{n}(c_i^1 - c_i^2)^2},$$

where c^1 and c^2 are the vectors that specify the distance from the coastline to the georeferenced line in each part of the beach. An example is provided in Figure 4.3. This plot can be accessed in a cloud folder linked in the Appendix for every extreme event detected in observed AWAC data.

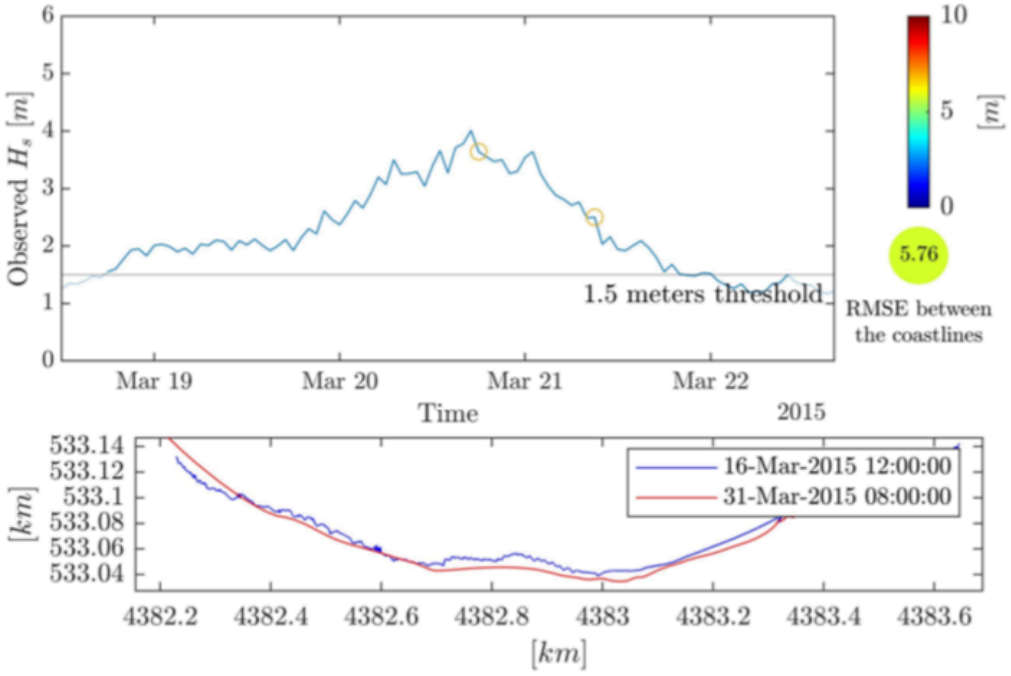

Fig. 4.3. Extreme event 18-Mar-2015 to 22-Mar-2015. Upper left plot includes the Hs observed during the event. The yellow circles indicate that the AWAC instrument provided an Error Code different from 0 at that time. On the upper right part, quantified impact. Lower panel: previous and following shorelines to the event, with dates specified in the legend.

4.5 Exposed and damaged elements

To complement the beach erosion data, the newspaper archives of the Diario de Mallorca and Última Hora have been exploited, for the period 2011-2022. From the list of storms obtained in the AWAC time series, a search has been developed in which the following variables are taken: if there is news about the event, if it cites Cala Millor, the typology of the damages following Jiménez et al. (2012):

- Low (1): some loss of sand, beach inundation and accumulation of sand and objects before the promenade, destruction of beach furniture.
- Medium (3): some erosion (without details), promenade inundation, accumulation of sand in the promenade, damage but unspecified.

- Maximum (5): meters of erosion or beach completely disappeared, inundation of houses, roads, etc; sand accumulation landward of the promenades, infrastructure destruction.

5. RESULTS

This section contains the results of the analyses of ocean and atmospheric data used to characterize the wave climate, obtained applying the methodology explained in Section 4. We first describe the mean wave climate at the local scale in Cala Millor on the basis of observations and modeled wave data. Secondly, we document and describe the extreme events that are later used to characterize the regional patterns in the Western Mediterranean oceanic and atmospheric fields. Finally, we evaluate the coastal impacts of the extreme events in terms of observed shoreline changes and their translation to the impact on exposed elements.

5.1 Cala Millor wave climate

The time series of wave parameters at Cala Millor are used to describe the local wave climate. We use both observed and modeled wave records.

5.1.1. Observed wave data

Figure 5.1 represents the entire observed wave record in the form of a wave rose. In terms of Tp, the maximum and minimum observed values are 13.63s and 1.71s, respectively. Across all directions, 99% of the observations exhibit a significant wave height of 3m or less, with maximum values exceeding 5m.

Peak direction (Dp) ranges from 60 to 120 degrees (nautical convention), corre-sponding NE-E and SE-E directions. This spectrum of directions is strongly influenced by the geographical configuration of the bay and the protection exerted by the local topographic features of Cap Vermell and Punta de n'Amer (see Fig. 2.1). This is also the cross-shore direction, in response to wave refraction by the bathymetry, thus controlling cross-shore transport processes in the beach.

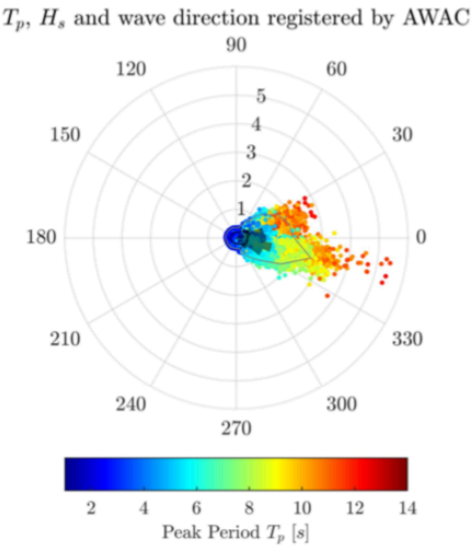

Fig. 5.1. Wave rose of in situ data measured by the AWAC instrument. Each point represents an observation. The position determines the direction (Dp) and significant wave height (Hs). The distance from the center represents the Hs and the color is the peak period. The gray line is located at the 99th percentile of Hs for each direction.

The time series of wave parameters are plotted in Figure 5.2. Here, in addition to the observed records, the extreme events are highlighted in red. We find that extrema with Hs exceeding 1.5m have peak period values over 4s, and occur primarily in directions close to zero (i.e., from the east). Note that recorded events are seasonally distributed, taking place predominantly between October and March.

In the observed period, 79 events have exceeded the 1.5m threshold, and amongst them we find the remarkable Storm Gloria in January 2020, corresponding to the maximum Hs in the record. This was an exceptional event that caused record-breaking waves along the eastern coasts of the Iberian Peninsula (Gulf of Valencia) and in the Balearic Islands, as well as heavy precipitation and flooding (Amores et al., 2020). In the eastern coast of Mallorca, Storm Gloria generated waves that caused overtopping on 15m high cliffs of Portocolom, meaning that estimated Hs should be at least 7m at this location (Amores et al., 2020).

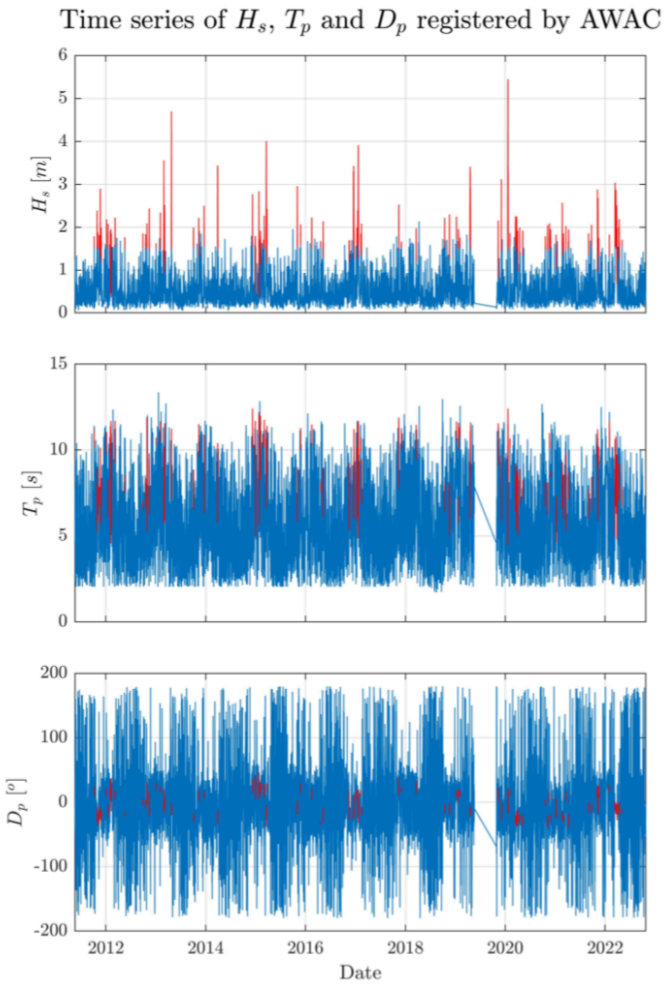

Fig. 5.2. Wave observations from in situ AWAC. Extreme events are identified in red.

5.1.2. Comparison between in-situ observations and hindcast

In order to work with the longer time series generated with the numerical model, these must be first compared to observations to ensure their consistency. The model outputs have already been validated at the regional scale, as mentioned in the data chapter. Nevertheless, we have

performed an additional validation in nearshore waters in Cala Millor. This is partly justified because we target local extreme events in this work and also because the overall validation of the modeled waves has been carried out in deep waters. Figure 5.3 illustrates the mesh closer to Cala Millor shore where hindcast data are available. The node of the mesh closer to the AWAC is labeled as the mesh Element #102. From now on, when working with Cala Millor modeled data, these will refer to this node of the mesh.

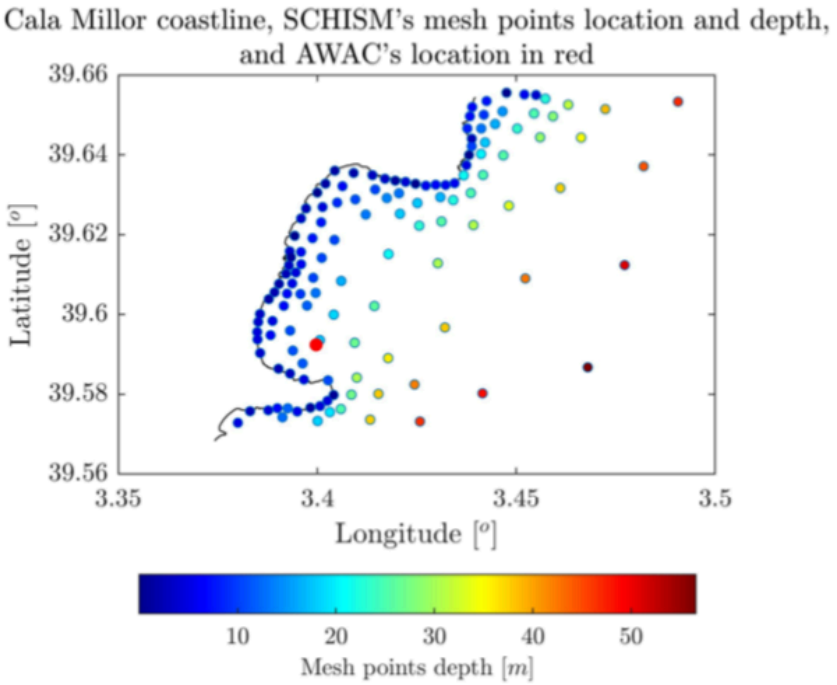

Fig. 5.3. Local nodes where there's wave data provided by the hindcast. The red dot indicates the location of the AWAC instrument.

Figure 5.4 compares observed and modeled Hs for their overlapping period. A visual inspection proves that hindcast data aligns well with observed data. This is confirmed by their correlation coefficient of 0.87. Nonetheless, extreme events are slightly underestimated by the model.

The wave peak direction is represented in Figure 5.5 using circular histograms for both sets of data. Note that, as mentioned in the description of the model, the output time series have a spectral resolution of 15º in wave peak direction. Although the dominant wave direction coincides, the spread in the model direction (right panel) is larger than in the observations (left panel). This can be partly explained by the much coarser spectral resolution in the model.

The comparison of the peak period (Tp) is shown in Figure 5.6. Both observed and modeled values are within the same range, showing a good model fit. We find, however, slightly different distributions in the most common Tp values.

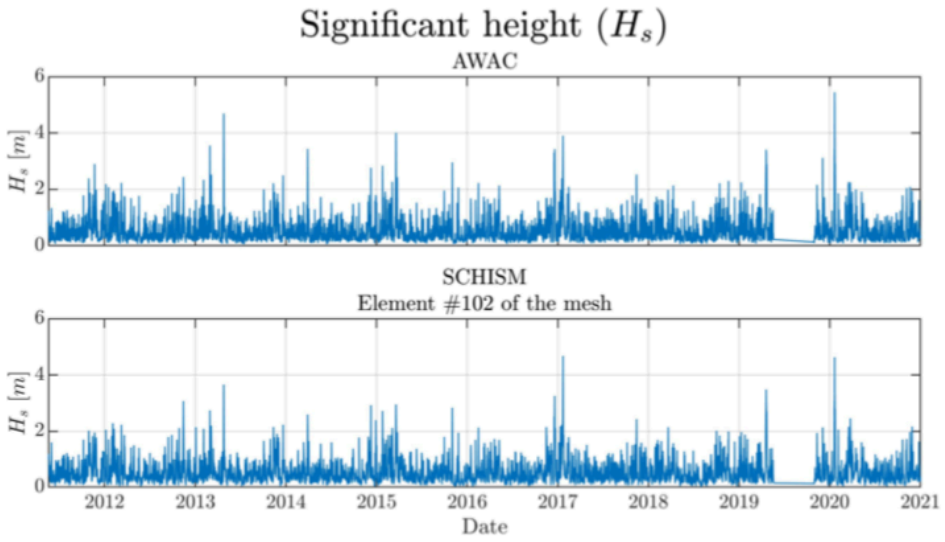

Fig. 5.4. Significant wave height time series of observed and modeled wave data.

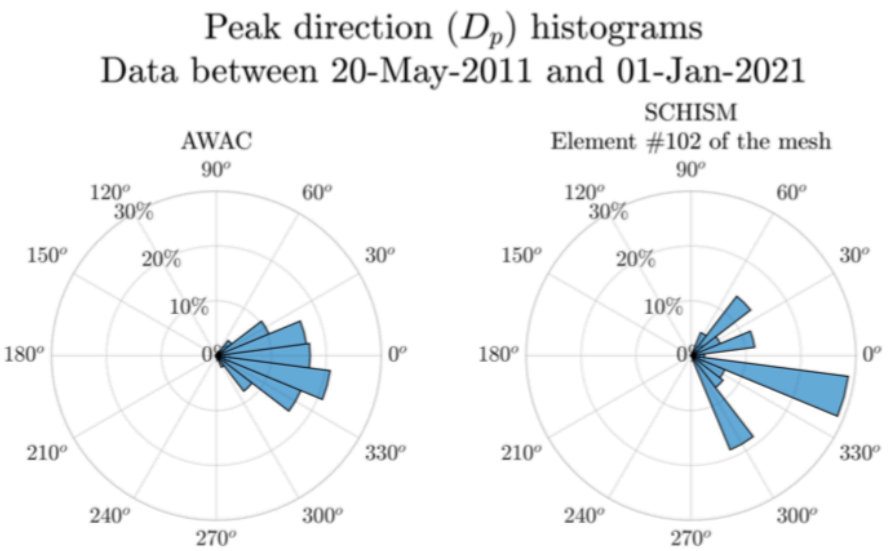

Fig. 5.5. Histograms of wave peak direction of observed (left) and modeled (right) wave data.

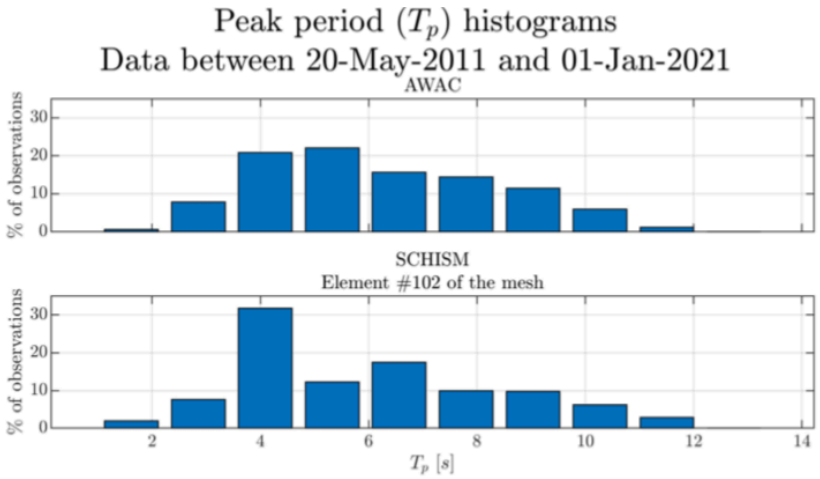

Fig. 5.6. Histograms of wave peak period histograms of observed (upper panel) and modeled (lower panel) wave data.

Modeled data are also represented in a wave rose, as we did above for the observations. Figure 5.7 includes the values of the hincasted data for the same period of the observed data. Again, we find that the resolution is 15° limits the representation of the data.

Overall, the comparison between observed and modeled wave parameters reveals that Hs is underestimated by the model, likely because winds in the forcing fields are also weaker than real winds (we recall that the resolution of the forcing is 0.25° in latitude and longitude). The modeled data is limited in terms of direction because of the relatively coarse spectral resolution, whereas it provides a good representation of Tp. All in all, modeled data constitutes a good representation of the wave climate at Cala Millor, and also provides a regional characterisation of wave climate.

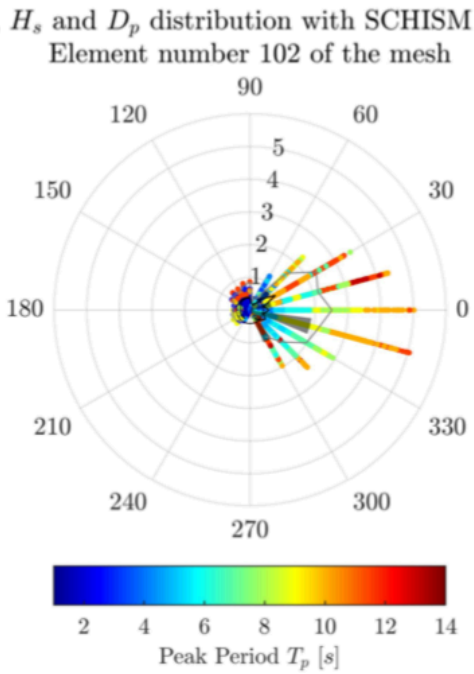

Fig. 5.7. Wave rose of modeled data for the period 2011-2022.

5.2 Characterisation of extreme wave events

The first characterisation of the 79 extreme events is provided in Figure 5.2. There is a clear seasonal character of the occurrence of extreme events, with most of them happening between the months October and March. The mean Hs during the events is 1.86 m, with the minimum value of 0.36 m and maximum 5.45 m, and a mean variance of 0.32 m. As for peak periods during the extreme events the mean value is 9s, ranging between 4.48 s and 12.42 s, with a variance of 2.4 s. The mean direction for these events is −3.77º, being the eastern (cross-shore) direction, the one that dominates the events.

To explore the common features of observed extreme events, we represent the temporal evolution of Hs with normalized values in Figure 5.8. The outcome of this analysis reveals a considerable dispersion in terms of duration. The median duration of the extreme events is 27 h, but with a very wide range between 6-380 h. Also, the temporal evolution of the extremes is very heterogeneous. Some events peak quickly at their maxima, while others maintain large Hs during

several hours. Figure 5.8 therefore indicates very diverse behavioral patterns of the extreme events.

The last metric used to characterize extreme events is the computation of return levels. We have fitted a selected set of extreme Hs to a Generalised Pareto Distribution (GPD). We have used observed records and also modeled extreme events, as these provide a much larger data sample that reduces the uncertainties in the fitting of the GPD to the empirical distribution of extremes. As explained in the methods, we employ an average of 2 events per year, to ensure that all events are actual extrema. Results for return periods up to 100 years are plotted in Figure 5.9. As previously pointed out, model outputs systematically underestimate extreme values, and this reflects in that the curve fitted to modeled data results in lower Hs than the one fitted to observed data. The distance between curves is substantial and the results of observations and modeled extremes are outside the confidence bounds. This result highlights the limitations of the regional model when used in local studies and calls for caution when interpreting coastal extreme waves in the nearshore.

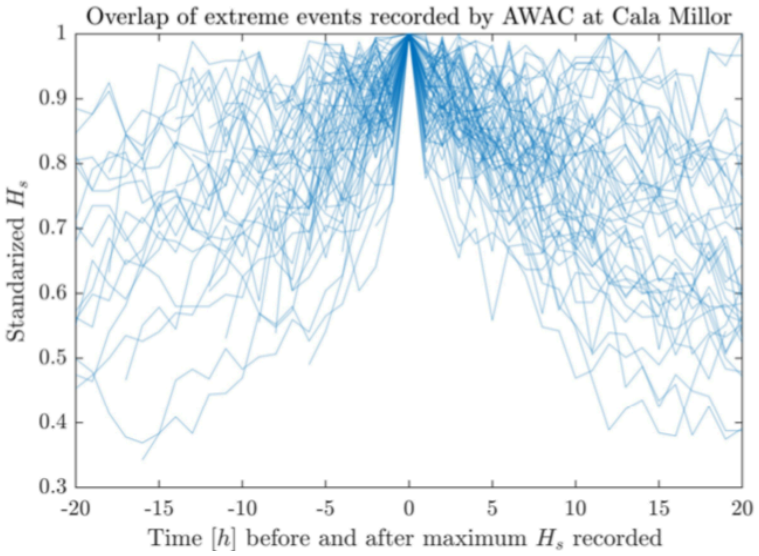

Fig. 5.8. Normalized (with values between 0 and 1) Hs during observed extreme events. Central time corresponds to maximum Hs.

5.2.1. Clustering of extreme events: Empirical Orthogonal Functions analysis.

This method has been applied to classify the regional patterns of extreme events identified in both the observations and the model. The number of fields included in the analyses is 75 for observed extreme events and 688 for the modeled events. The results are presented in Figures 5.10 and 5.11 and include the time series and the spatial patterns associated with each EOF. Despite the large difference in the number of events, and the limitations of the hindcast data (see section above), it is noteworthy the consistency between the two EOF results.

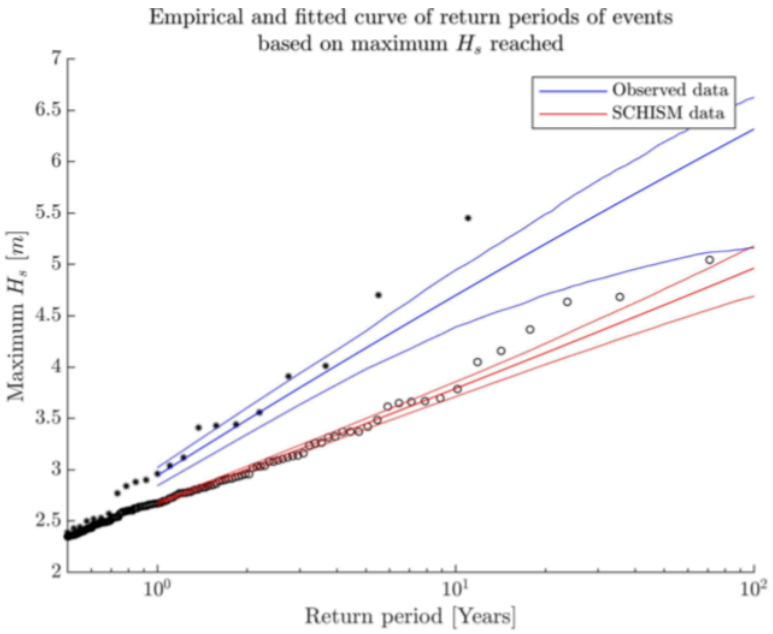

Fig. 5.9. Results of applying return period methodology to observed and modeled data. Star shapes correspond to the empirical distribution obtained with observed data, while circles correspond to the empirical distribution obtained with modeled data. Same happens with blue and red, respectively.

In both cases, the analyses show one dominant pattern representing 68.28 and 57.79% of the variance in observed and modeled events, respectively. This first EOF is characterized by large Hs values in the central Western Mediterranean, coinciding with the region of strongest winds blowing from the Gulf of Lions. EOF2 displays a dipole-like structure in the E-W direction, and explains a much smaller amount of variance (around 10%). EOF3 shows marked differences between the Northern African and Tyrrhenian Sea, likely linked to winds blowing from the E direction. The EOF4 pattern has a N-S dipole-like structure and an explained variance of ~5%. This pattern identifies incoming waves from the northern part of the basin that could be partly explained by perturbations generated in the Gulf of Genoa. EOF5 is also included but in both cases displays a noisy pattern and is responsible for a very small amount of variance of only ~2%. It is important to note that, for the dominant patterns, the location of CLM is within a gradient zone.

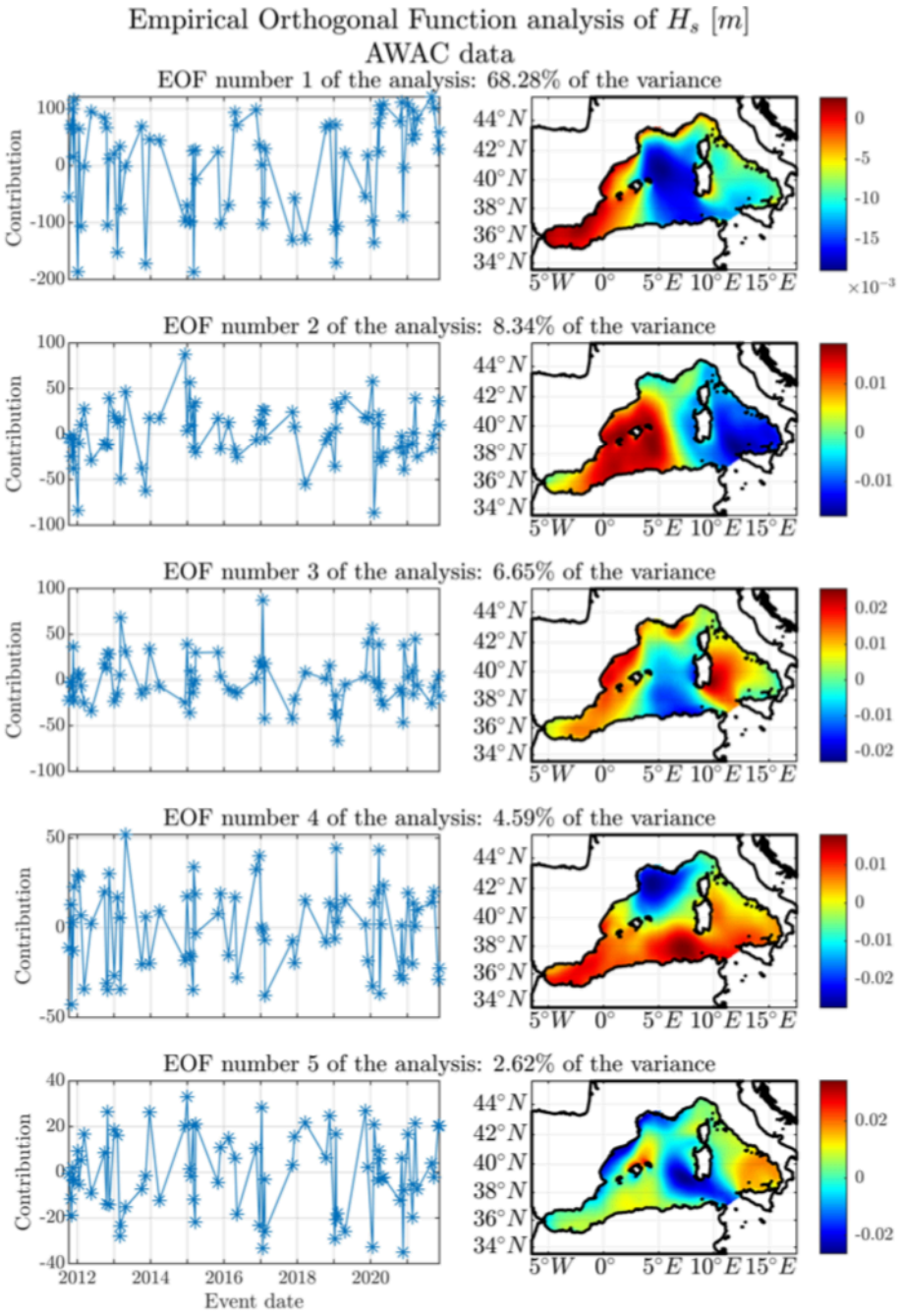

Fig. 5.10. EOF analysis on Hs fields corresponding to observed extreme events at Cala Millor. On the left, time series associated with each EOF (note that x-axis is the timing of the events). On the right, the EOF spatial patterns.

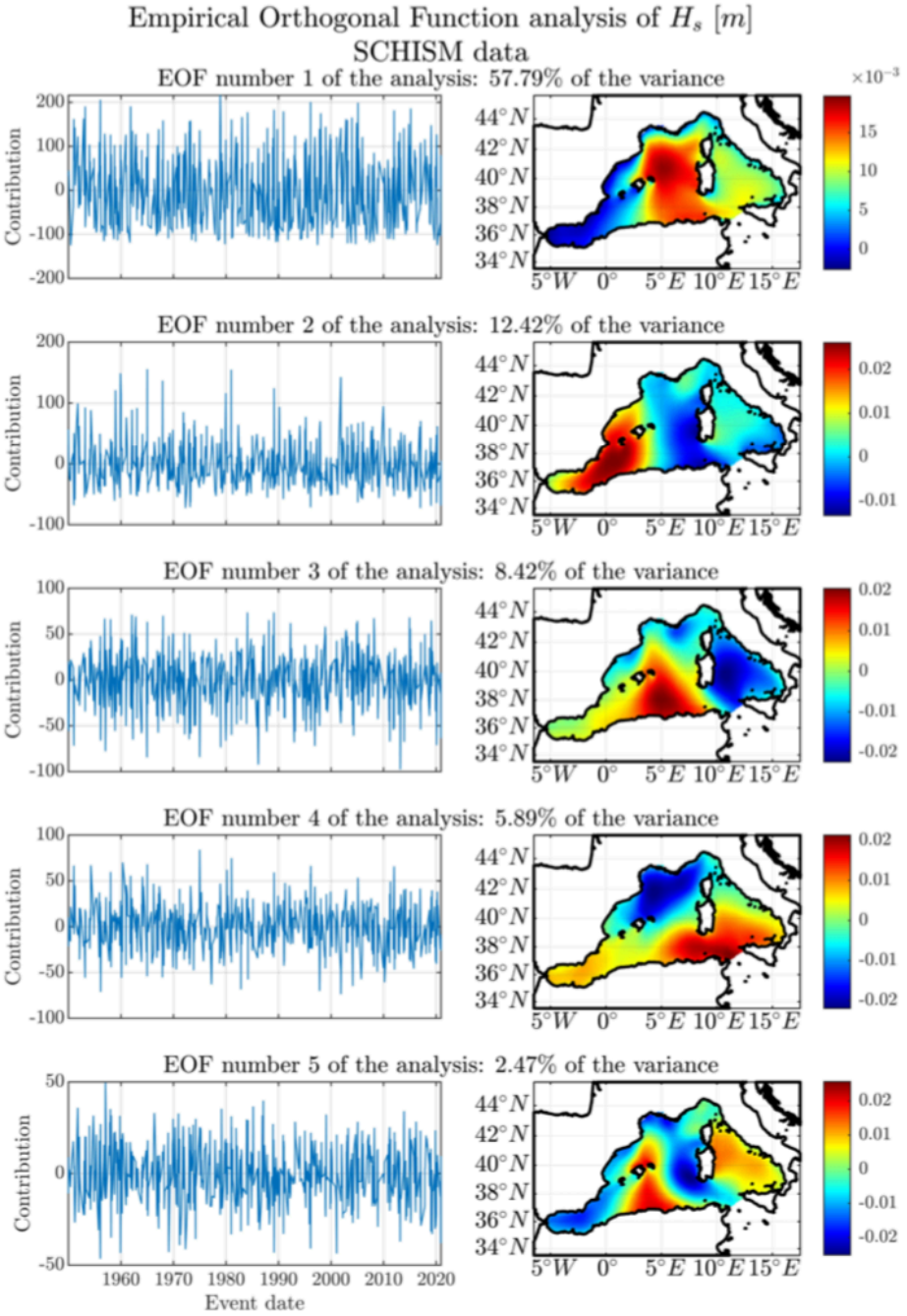

Fig. 5.11. EOF analysis on Hs fields corresponding to modeled extreme events at Cala Millor. On the left, time series associated with each EOF (note that x-axis is the timing of the events). On the right, the EOF spatial patterns.

5.2.2. Clustering of extreme events: K-means analysis.

The K-means algorithm is generally used in large data sets to reduce dimensionality. Here, we have restricted the application of this approach to the modeled data, with 688 fields. The use of K-means implies the choice of a prescribed number of clusters. To avoid a subjective choice to the extent possible, we have run the algorithm with a range of clusters, from 1 to 10, and calculated a

metric of the uncertainties. Specifically, for each value of the number of clusters, we calculate the sum of the euclidean distances of every element within the cluster with respect to their corresponding centroid. Figure 5.12 represents this error as a function of the number of clusters. The choice of the final number is one that substantially reduces the uncertainty with respect to lower values (the so-called "elbow method"). In our case the final choice was 4 clusters.

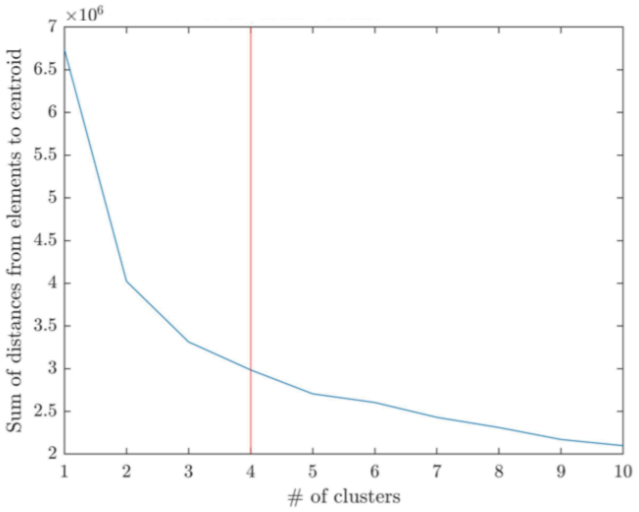

Fig. 5.12. Uncertainty of K-means clustering technique measured as the euclidean distance between the elements within each cluster and their corresponding centroid. The number of 4 clusters is the final choice (red vertical line).

The total number of modeled extremes were therefore classified into 4 clusters. Then, we have generated composite maps of the mean atmospheric and oceanic patterns for each cluster. The atmospheric maps correspond to surface wind fields 12h before maximum Hs was recorded at CLM. The oceanic maps correspond to Hs and D_p wave fields simultaneously to the maximum Hs at CLM. The composites are the averages of the atmospheric and oceanic fields for all extreme events within the same cluster. They represent the regional patterns that lead to local extremes in Cala Millor. The composite maps resulting from the K-means clustering are plotted in Figures 5.13, 5.14, 5.15 and 5.16.

Cluster 1 in Figure 5.13 represents over 41% of the events and presents winds and waves marked by their easterly direction, with winds reaching up to 9.3 m/s and Hs of up to 2.55 m. The second cluster, mapped in Figure 5.14, is linked to 22% of the events. The regional pattern in this cluster has a clear northern component, with winds blowing from the N and NW from the Gulf of Lion. Surface winds reach 17.45 m/s, driving waves up to 5.1 m in Hs. The cluster 3 in Figure 5.15 accounts for over 23% of the events and is associated with atmospheric perturbations from the NE of the basin, likely generated in the Gulf of Genoa. Mean surface winds reach 12.1 m/s and waves 4 m of Hs. Finally, cluster number 4 presents many characteristics similar to number 2, with a dominant pattern from the N, N-W, and strong surface winds from the Gulf of Lions. This matching between both patterns indicates that there are likely minor differences between selecting 3 or 4 clusters to represent the regional patterns responsible for extreme events in Cala Millor.

Our results indicate that the K-means clustering identifies 3 different and independent regional atmosphere-ocean situations that cause extreme wave events occurring in CLM. These

correspond to 1) atmospheric perturbations generated in the central-east Mediterranean basin, traveling from the E and generating waves that impact directly in the East coast of Mallorca (cluster 1); 2) strong surface northerly winds blowing from the Gulf of Lions, that turn out to be the most common (clusters 2 and 4); and 3) atmospheric perturbations generated in the Gulf of Genoa with winds from the NE in the western basin and large waves reaching the east coasts of the Balearic Islands, favored by the relatively long fetch (cluster 3).

Although the K-means results are robust in terms of the spatial patterns, the number of events associated with each of them varies with different realizations. This is an inherent limitation of the approach, as the outputs may differ depending on the initial conditions. Nevertheless, the fact that the patterns are stable and associated with known atmospheric situations, leads us to consider the classification reliable.

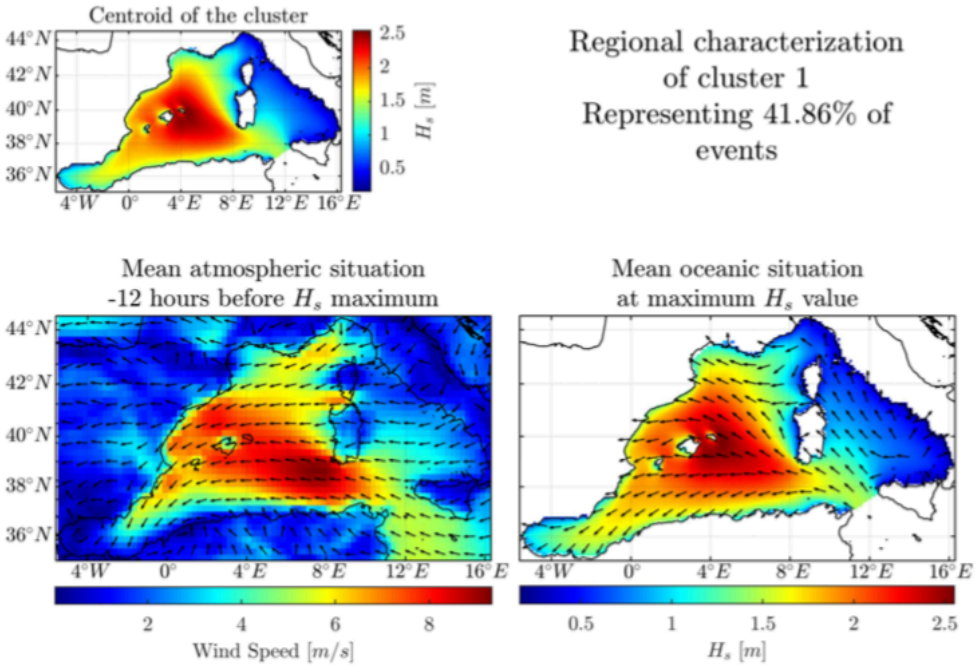

Fig. 5.13. Fields associated with the cluster number 1, representing 41.86% of the extreme events detected 1950-2021. Upper left panel: centroid of the cluster, defined by regional Hs data. Lower left panel: mean atmospheric situation 12h before maximum Hs, color indicates wind speed and arrows represent wind direction. Lower right panel: mean oceanic situation at maximum Hs, color indicates Hs and arrows represent Tp .

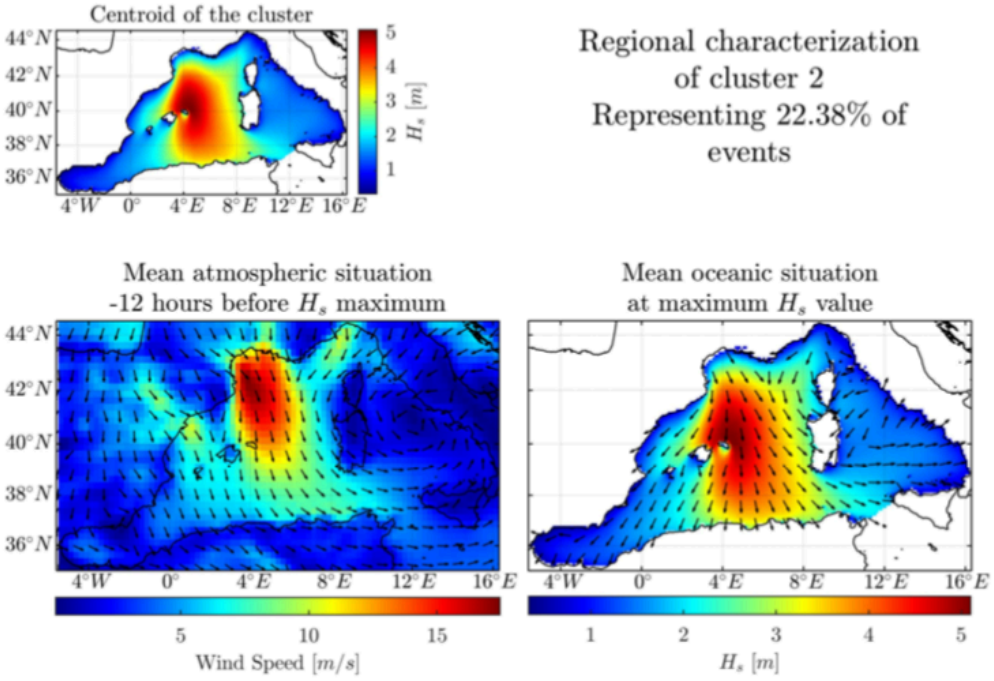

Fig. 5.14. Fields associated with the cluster number 2, representing 22.38% of the extreme events detected 1950-2021.

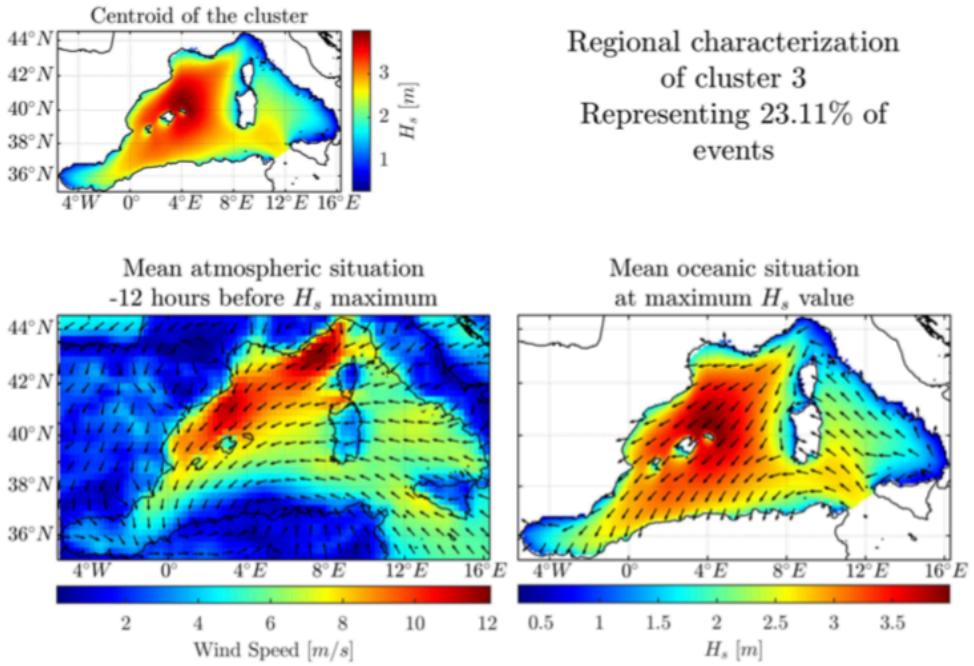

Fig. 5.15. Fields associated with the cluster number 3, representing 23.11% of the extreme events detected 1950-2021.

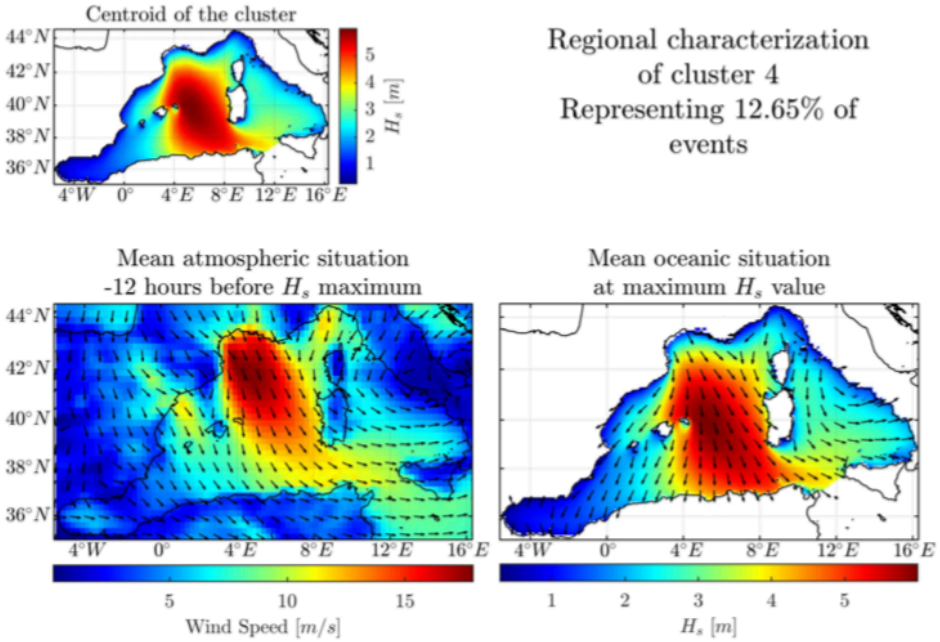

Fig. 5.16. Fields associated with the cluster number 4, representing 12,65% of the extreme events detected 1950-2021.

5.3 Impact of extreme wave events on beach shoreline

According to the wave observations in CLM, extreme wave events are common features that occur systematically every winter, triggered by atmospheric perturbations that can be either generated in different parts of the basin (Gulf of Genoa and central Mediterranean) or traveling from the Gulf of Lions. In any of these situations, local Hs can exceed 1.5-2m. Observed extreme events in Hs are above 5.5 m in the entire record, and return levels result in ~ 5m for a 10-year period. The exposure of Cala Millor beach to incoming waves is therefore large. We thus evaluate the impact that these extreme events have on the beach dynamics using the simultaneous in-situ wave measurements and the observations of shoreline position. We anticipate that the shoreline response of the beach may depend on individual storms but also on the occurrence of storm groups, as the changes can be linked to the initial state of the beach and to former impacts (Morales-Márquez et al., 2018). We consider waves as the only forcing mechanisms in the beach response. Despite being the dominant forcing factor, we remark that we are not accounting for mean sea level changes or storm surges.

We seek a relationship between the shoreline impact and the accumulated energy of every storm (i.e., energy integrated during the extreme event). The total number of events that we have used is 79. The results are plotted in Figure 5.17. To identify joint and isolated events we have color-coded each event depending on the number of events recorded in the previous 45 days. We find that the events that cause shoreline changes larger than 7 m are, in most cases, either very energetic events or group events or both. However, there is one exception. Also, there are energetic events and groups of events without significant impact.

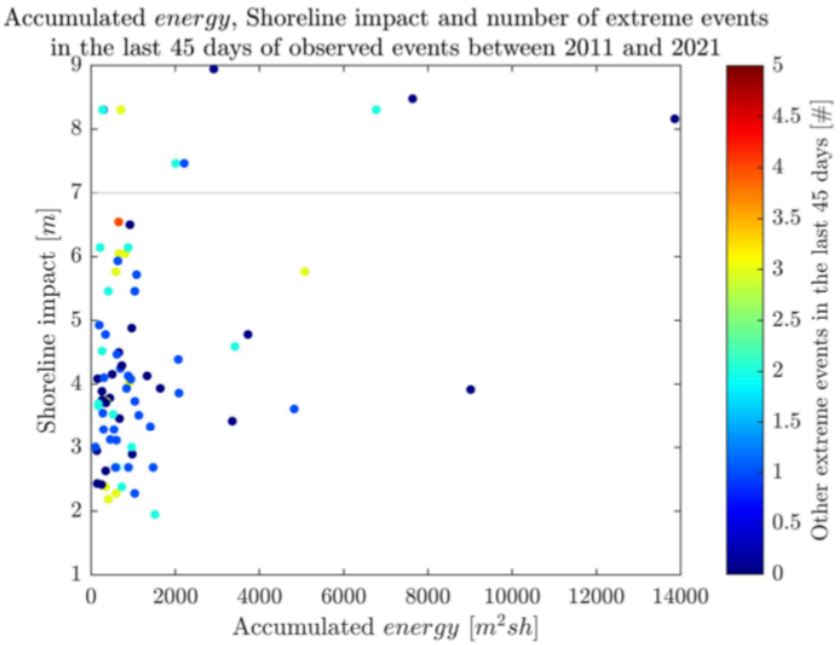

Fig. 5.17. Shoreline impact and accumulated energy during the event. The color represents the number of other events in the last 45 days.

To improve the visualization, we have plotted the accumulated energy and shoreline changes over time in Figure 5.18, where every point represents one extreme event. Note that only shoreline positions before and after every event are included here, rather than the entire time series. This figure indicates that large changes in the shoreline position (green dots) occur often associated with energetic events (red dots). It also shows that the grouping of events may trigger a large shoreline change with moderate events. Particular cases and behavior are described in detail in the following:

- December 2016 and January 2017: two events better understood together, high energy and high impact. The first event lasted from 16th to the 21st of December, with maximum Hs of 3.43 m and impact of 3.61 m. The second one, from 26th to the 23rd of January, with maximum Hs of 3.91 m and impact of 8.3 m. Both of them present a regional pattern of the Cluster 1 (K-means).
- March 2022: the longest event recorded, lasting more than 15 days, from the 14th to the 30th. Highest Hs of 3 m and remarkable impact of 8.16 m. Also high accumulated energy and high impact.
- April 2019: lasting from the 18th to the 23rd. Maximum Hs reaching 3.41 meters and impact on the shoreline of 8.47 m. The regional pattern fits the Cluster 1. Preceded by three extreme events in January and one in February of the same year.
- March 2014: the event lasted from the 28th to the 30th. With a maximum Hs observation of 3.44 m, and a resulting change in shoreline of 8.94 m, the maximum value of observed change in shoreline associated with an extreme event. The regional situation identifies with Cluster 1 of the K-means analysis, with winds and waves impacting directly on the shore. No extreme event has been detected in the previous 45 days, and it is not especially energetic, but inflicted a great impact.

- January 2020: Storm Gloria extreme event lasted from 19th to the 23rd. With the maximum Hs observed, 5.45 m, and an impact of 3.92 m. The regional pattern identifies with Cluster 1 on the K-means analysis. The event was highly energetic, but the quantified impact is rather low.

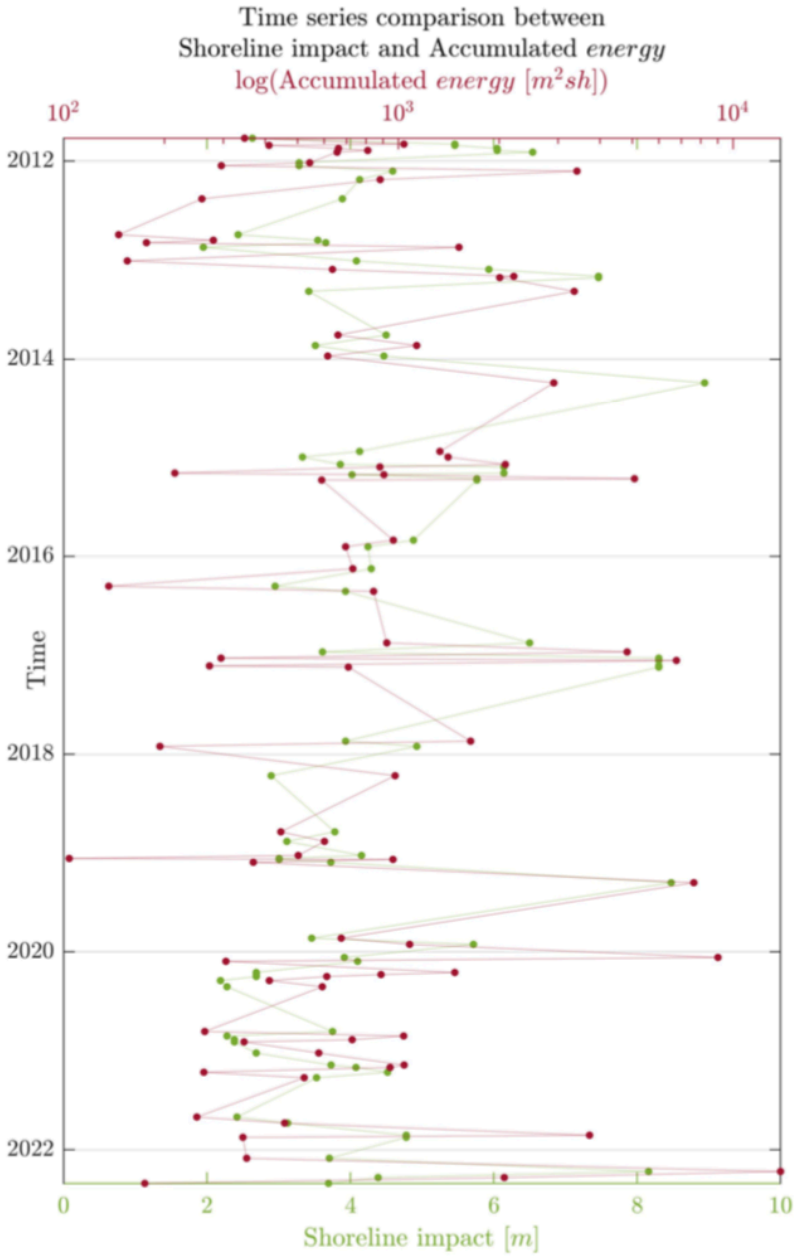

Fig. 5.18. Time series of shoreline impact and accumulated energy. Every point represents an observed extreme event. Note the logarithmic scale in accumulated energy.

5.4 Storm-induced damage and exposed elements

The first characterisation of storm-induced damages from the 79 extreme events obtained from the AWAC wave time series is provided in Figure 5.19. On average, the storms represent an average setback of the coastline of 4.4 m, with minima of 1.3 and maxima of 8.9 m of average retreat of the dry beach. In about 50% of the cases the retreat of the coastline does not exceed

4m on average, which is within the range of natural variability of the beach coastline. Even if RMSE values lower than 6m are considered, ca. 80% of the events would still continue within the oscillations of the system. However, these values can be critical depending on the area of the beach, since in the southern area the outcropping of rocky elements makes it difficult for recreational use of the beach and the recovery of the beach profile. Only 9% of events represent an average loss of the coastline of 9m inland. These are the cases with the greatest impacts on the beach, with loss of volumes of sand and damage to beach furniture (lifeguard towers, cleaning points, accesses, etc.) (Fig. 5.20).

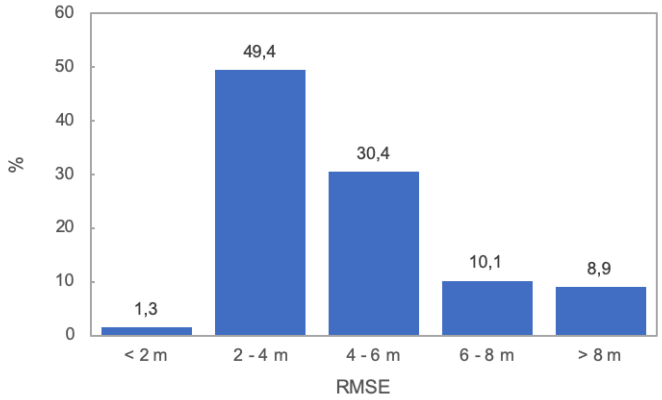

Fig. 5.19. Histogram of the RMSE of the dry beach associated with storms characterized from the AWAC wave time series.

During the 2011-2022 period, the most damaging storms for the beach have been in April 2014 (RMSE = 8.9 m), January 2017 (RMSE = 8.3 m), April 2019 (RMSE = 8.5 m) and March 2022 (RMSE = 8.2 m).

Given the absence of systematic technical reports from local administrations and the possibility of comparing them and evaluating the impacts, a systematic analysis of the press news related to CLM has been used. This approach has not been successful because although the newspapers report episodes of heavy rain and flooding, they barely pay attention to the beach except for the capsize of a boat or the death of a beach user swept away by rip currents or a heart attack. When Cala Millor appears in the press, it does so because the stakeholders are promoting actions to improve or recover the beach, but not as a result of a specific storm, but rather a tendency to recede in some sectors of the beach (Fig. 5.21).

Fig. 5.20. Impact of April 2019 extreme sea storm at CLM. Being one of the most energetic storms from the characterized period, the damage relates with sand transport and accumulation, and accumulation of objects before the promenade.

'Gloria' deja una estela de devastación en Cala Rajada, Cala Millor y s'Illot

El paseo de Cala Gat se hundió y quedó intransitable - El vendaval se llevó media playa y destruyó un árbol centenario en Cala Millor - Vecinos de s'Illot limpiaron la primera línea

Biel Capó - son servera

23·01·20 | 02:48

El Llevant ha vuelto a ser **noqueado por otro violento fenómeno meteorológico**. La borrasca Gloria ha dejado un rastro de d**evastación en Cala Rajada, Cala Millor y s'Illot**. El peor temporal marítimo que se recuerda en años en la zona ha causado **daños millonarios en infraestructuras públicas, negocios, viviendas particulares y en embarcaciones** que quedaron a merced de gigantescas olas.

La primera línea de estos núcleos costeros ayer amaneció **cubierta de un manto de suciedad, plásticos, algas y piedras** que el mar escupió con furia el pasado martes. Vecinos y trabajadores empezaron las **árduas tareas de limpieza ayudados de mangueras, palas y escobas**. Gloria por fin dio una tregua en la isla y el temporal amainó.

PUBLICIDAD

Nuevo BMW iX2.

BMW

Más información

Súbete a bordo del nuevo Alfa Romeo Stelvio

Alfa Romeo

Haz clic aquí

Ultima Hora

Iniciar sesión

Regístrate

Noticias | Part Forana Sant Llorenç Son Servera

Costas dará respuesta en 15 días a la regeneración de la playa de Cala Millor

El consorcio turístico se reunió con el Ministerio de Transición Ecológica

8M Dia Internacional de les Dones

Ajuntament de Palma

És Igualtat

La playa, sobre todo en la zona de Cala Nau, ha perdido mucha arena. | **Redacción Part Forana**

Assumpta Bassa | Cala Millor, Son Servera | 13/05/22 3:59

Fig. 5.21. Examples of the appearance and treatment of CLM in the written press and the elements exposed to the action of the storms. The upper block shows a detail of the impacts of storm Gloria on the beach that appeared in the Diario de Mallorca on 01/23/2020 and in the lower block, the recurring news related to the demand by local sectors for a regeneration of the beach in the Ultima Hora of 05/13/2022.

BIBLIOGRAPHY

Álvarez-Ellacuría, A., Orfila, A., Gómez-Pujol, L., Simarro, G., Obregón, N. 2011. Decoupling spatial and temporal patterns in short-term beach shoreline response to wave climate. Geomorphology, 128, 199-208.

Amores, A., Marcos, A., Carrió, D.S., Gómez-Pujol, L. 2020. Coastal impacts of Storm Gloria (January 2020) over the north-western Mediterranean. Nat. Haz. Earth Sys., 20, 1955–1968.

Calafat, F.M., Gomis, D., 2009. Reconstruction of Mediterranean sea level fields for the period 1945e2000. Global Planet. Change 66 (3e4), 225e234. https://doi.org/10.1016/j.gloplacha.2008.12.015.

Callaghan, D.P., Ranasinghe, R., Short, A.D. 2009. Quantifying the storm erosion hazard for coastal planning. Coast. Eng., 56, 90-93.

Cañellas, B., Orfila, A., Méndez, F.J., Menéndez, M., Gómez-Pujol, L., Tintoré, J. 2017. Application of a POT model to estimate the extreme significant wave height levels around the Balearic Sea (Western Mediterranean). Journal of Coastal Research, SI 50, 329-333.

Castelle, B., Harley, M. 2020. Extreme events: impact and recovery. In: Jackson, D.W.T. and Short, A.D. (eds.), Sandy Beach Morphodynamics. Elsevier, Amsterdam, pp. 535-556.

Castelle, B., Marieu, V., Bujan, S., Splinter, K.D., Robinet, A., Sénéchal, N., Ferrerira, S. 2015. Impact of the winter 2013-2014 series of severe Western Europe storms of a double-barred sandy coast: beach and dune erosion and megacusp embayments. Geomorphology, 238, 135-148.

Castillo, E., Hadi, A.S.. 1997. Fitting the generalized pareto distribution to data. J. Am. Stats. Ass., 92, 1609–1620.

Cooper, J.A.G., Jackson, D.W.T., Navas, F., McKenna, J., Málvarez, G. 2004. identifying storm impacts on an embayed, high-energy coastline: examples from western Ireland. Mar. Geol., 210, 261-280.

Dean, R.G., Dalrymple, R.A. 1991. Water Wave Mechanics for Engineers and Scientists. World Scientific Publishing, New Jersey. 354 pp.

Fernández-Mora, A., Criado-Sudau, F.F., Gómez-Pujol, L., Tintoré, J., Orfila, A. 2023. Ten years of morphodynamic data at a microtidal urban beach: Cala Millor (Western Mediterranean Sea). Scientific Data, 10, 301, doi: 10.1038/s41597-023-02210-2.

Gómez-Pujol, L. 2014. Observacions a propòsit de la brisa de mar estival al Llevant de Mallorca (Illes Balears). Boll. Soc. Hist. Nat. Balears, 57, 181-201.

Gómez-Pujol, L., Orfila, A., Álvarez-Ellacuría, Tintoré, J. 2011. Controls on sediment dynamics and medium-term morphological change on a barred microtidal beach (Cala Millor, Mallorca, Western Mediterranean). Geomorphology, 132, 87-98.

Guisado-Pintado, E., Jackson, D.W.T. 2018. Multi-scale variability of storm Ophelia 2017: the importance of synchronized environmental variables in coastal impact. Sci. Total Environ., 630, 287-301.

Harley, M.D. 2017. Coastal storm definition. In: Ciavola, P., Coco, G. (eds.), Coastal Storms. John Wiley & Sons, Chichester, pp. 1-21.

Harley, M.D., Turner, I.L., Kinsela, M.A., Middelton, J.H., Munford, P.J., Splinter, K.D., et al. 2017. Extreme coastal erosion enhanced by anomalous extratropical storm wave direction. Scient. Rep. 7, 6033.

Hersbach, H., Bell, B., .Berrisford, P., Biavati, G., Horányi, A., MuñozSabater, J., Nicolas, J., Peubey, C., Radu, R., Rozum, I., Schepers, D., Simmons, A., Soci, C., Dee, D., Thépaut, J.N. 2023. Era5 monthly averaged data on single levels from 1940 to present. Copernicus Climate Change Service (C3S) Climate Data Store (CDS). 2.3, 5.

Hesterberg, T. 2011. Bootstrap. WIREs Computational Statistics, 3, 497–526.

Hoefel, F., Elgar, S. 2003. Wave-induced sediment transport and sandbar migration. Science, 299, 1885-1887.

Ibsen, M.I., Brunsden, D. 1996. The nature, use and problems of historical archives for the temporal occurrence of landslides with specific reference to the South coast of Britain. Ventnor, Isle of Wight. Geomorphology, 15, 241-258.

Infantes, E., Terrados, J., Orfila, A., Cañellas, B., Álvarez-Ellacuria, A. 2009. Wave energy and the upper depth limit distribution of *Posidonia oceanica*. Bot. Mar., 52, 419–427.

Jiménez, J.A., Sancho-García, A., Bosom, E., Valdemoro, H.I., Guillén, J. 2012. Storm-induced damages along the Catalan coast (NW Mediterranean) during the period 1958-2008. Geomorphology, 143-144, 24-33.

Kinsela, M.A., Morris, B.A.S., Limklater, M., Hanslow, D.J. 2017. Second-pass assessment of potential exposure to shoreline change in New South Wales, Australia, using a sediment compartments framework. J. Mar. Sci. Eng., 5, 61. doi: 10.3390/jmse5040061.

Marcos, M., Tsimplis, M.N., 2008. Coastal sea level trends in southern Europe. Geophys. J. Int. 175, 70e82. https://doi.org/10.1111/j.1365-246X.2008.03892.x.

Masselink, G., Austin, M., Scott, T., Poate, T., Russell, P. 2014. Role of wave forcing, storms and NAO in outer bar dynamics on a high-energy micro-tidal beach. Geomorphology, 226, 76-39.

McPhillips, L.E., Chang, H., Chester, M.V., De pietri, Y., Friedman, E., Grimm, N.B. et al., 2018. Defining extreme events: a cross-disciplinary review. Earth's Fut. 6, 441-455.

Mendoza, E.M.T., Jimenez J.L., Mateo, J. 2009. A coastal storm's intensity scale for the Catalan Sea (NW Mediterranean). Nat. Hazards Earth Syst. Sci. 11, 2453–2462.

Michelucci, U., Venturini, F. 2021. Estimating Neural Network Performance With bootstrap: A tutorial. Machine Learning and Knowledge Extraction, 3, 357–373

Morales-Márquez, V. Orfila, A., Simarro, G., Gómez-Pujol, L., Álvarez-Ellacuría, A., Conti, D., Galán, A., Osorio, A.F., Marcos, M. 2018. Numerical and remote techniques for operational beach management under storm group forcing. Nat. Hazards Earth Syst. Sci., 18, 1-13.

Morales-Márquez, V., Orfila, A., Simarro, G., Marcos, M. 2020. Extreme waves and climatic patterns of variability in the eastern North Atlantic and Mediterranean basins. Ocean Science, 16, 1385–1398.

Nieto, M.N., Garau, B., Balle, S., Simarro, G., Zarruk, G.A., Ortiz, A., Tintoré, J., Álvarez Ellacuría, A., Gómez-Pujol, L., Orfila, A. 2010. An open source, low cost video-based coastal monitoring system. Earth Surf. Process. Land., 35, 1712–1719.

Orfila, A., Jordi, A., Basterretxea, G., Vizoso, G., Marbà, N., Duarte, C.M., Werner, F.E., Tintoré, J. 2005. Residence time and *Posidonia oceanica* in Cabrera Archipelago National Park, Spain. Continental Shelf Research, 25, 1339-1352.

Sancho-García, A., Guillén, J., Gracia, V., Rodríguez-Gómez, A.C. 2021. The use of news information published in newspapers to estimate the impact of coastal storms at a regional scale. J. Mar. Sci. Eng., 9, 497.

Sénechal, N., Castelle, B., Bryan, K.R. 2017. Storm clustering and beach response. In: Ciavola, P., Coco, G. (eds.), Coastal Storms. John Wiley & Sons, Chichester, pp. 151-174.

Tintoré, J., Medina, R., Gómez-Pujol, L., Orfila, A., Vizoso, G. 2009. Integrated and interdisciplinary scientific approach to coastal management. Ocean. Cost. Manag., 52, 493-505.

Toimil. A., Losada, I.J., Díaz-Simal, P., Izaguirre, C., Camus, P. 2017. Multi-sectorial, high-resolution assessment of climate change consequences of coastal flooding. Climatic Change, 145, 431-444.

Toomey, T., Amores, A., Marcos, M., Orfila, A. 2022. Extreme sea levels and wind- waves in the mediterranean sea since 1950. Front. Mar. Sci., 9, 991504. DOI: 10.3389/fmars.2022.991504

Young, A.P., Guza, R.T., O'Reilly, W.C., Burvingt, O., Flick, R.E. 2016. Observations of coastal cliff base waves, sand levels, and cliff top shaking. Earth Surf. Process. Land., 41, 1564-1573.

Zhang, Y. J., Ye, F., Stanev, E.V., Grashorn, S. 2016. Seamless cross-scale modeling with SCHISM. Ocean Modelling, 102, 64–81.

APPENDIX. Storms characteristics from AWAC records at Cala Millor.

Storm start	Maximum Hs time	Storm end	Duration	maxHs	tp_maxHs	meanHs	maxmaxH	meanTp	num_events45	max Energy	Totl energy
7/10/11 22:00	8/10/11 6:00	8/10/11 9:00	12	1,8	11,1	1,6	2,7	10,7	0,0	35,6	347,2
29/10/11 6:00	29/10/11 14:00	30/10/11 17:00	36	2,4	7,9	1,9	3,8	7,9	1,0	45,2	1039,3
3/11/11 2:00	3/11/11 15:00	3/11/11 21:00	20	1,9	7,7	1,7	3,0	7,3	2,0	27,1	410,8
14/11/11 9:00	14/11/11 19:00	15/11/11 17:00	33	1,8	6,8	1,7	3,3	7,2	3,0	25,6	662,3
21/11/11 20:00	21/11/11 22:00	22/11/11 22:00	27	2,9	8,9	1,8	4,1	8,8	3,0	75,0	810,4
28/11/11 1:00	28/11/11 6:00	29/11/11 9:00	33	2,0	7,3	1,6	3,3	7,4	4,0	28,9	656,3
6/1/12 9:00	6/1/12 13:00	6/1/12 23:00	15	2,2	10,5	1,9	3,4	10,4	1,0	50,4	543,5
17/1/12 7:00	17/1/12 11:00	17/1/12 18:00	12	2,1	8,0	1,8	3,1	7,6	1,0	34,5	296,0
2/2/12 21:00	7/2/12 6:00	10/2/12 13:00	185	2,0	10,4	1,3	3,0	10,0	2,0	40,1	3417,2
8/3/12 14:00	8/3/12 23:00	9/3/12 12:00	23	2,2	11,0	1,9	3,5	10,8	1,0	54,8	882,6
18/5/12 20:00	18/5/12 23:00	19/5/12 7:00	12	1,8	8,0	1,6	2,9	8,1	0,0	25,3	258,9
28/9/12 9:00	28/9/12 15:00	28/9/12 16:00	8	1,9	6,8	1,6	2,7	6,8	0,0	23,6	146,0
18/10/12 17:00	18/10/12 23:00	19/10/12 6:00	14	1,8	7,8	1,6	2,8	7,6	1,0	26,4	280,1
27/10/12 20:00	27/10/12 22:00	28/10/12 1:00	6	2,1	5,3	1,8	3,8	8,6	2,0	51,9	176,8
12/11/12 20:00	13/11/12 23:00	15/11/12 2:00	55	2,4	8,0	1,8	4,0	8,1	2,0	56,9	1517,5
3/1/13 4:00	3/1/13 7:00	3/1/13 9:00	6	1,6	10,5	1,6	2,5	10,4	0,0	27,8	155,0
3/2/13 8:00	3/2/13 14:00	3/2/13 23:00	16	2,3	11,5	1,9	4,2	11,2	1,0	63,2	635,6
28/2/13 2:00	28/2/13 19:00	2/3/13 6:00	53	3,6	9,4	2,1	5,8	8,8	1,0	119,4	2213,0
4/3/13 18:00	6/3/13 4:00	7/3/13 2:00	57	2,5	10,5	1,9	4,0	9,6	2,0	66,7	2008,7
24/4/13 20:00	25/4/13 12:00	26/4/13 13:00	42	4,7	10,5	2,7	8,3	9,4	0,0	231,3	3353,8
3/10/13 13:00	3/10/13 18:00	4/10/13 13:00	25	2,0	7,9	1,8	3,4	8,2	0,0	33,1	660,2
11/11/13 3:00	11/11/13 9:00	12/11/13 10:00	32	2,2	11,0	1,8	3,6	10,7	1,0	54,2	1134,4
20/12/13 8:00	20/12/13 12:00	20/12/13 20:00	13	2,5	10,4	2,1	3,9	10,1	1,0	65,1	615,1
28/3/14 20:00	29/3/14 16:00	30/3/14 20:00	49	3,4	9,5	2,5	5,1	8,9	0,0	117,6	2913,6
9/12/14 6:00	9/12/14 18:00	10/12/14 9:00	28	2,8	12,4	2,0	4,5	11,1	0,0	95,3	1331,0
28/12/14 20:00	29/12/14 9:00	1/1/15 11:00	88	1,8	10,4	1,2	2,9	9,7	1,0	36,6	1408,0
25/1/15 2:00	25/1/15 10:00	28/1/15 9:00	80	2,8	12,1	1,4	4,5	10,2	1,0	97,3	2087,8
4/2/15 13:00	5/2/15 7:00	6/2/15 0:00	36	1,9	11,6	1,5	3,0	11,1	2,0	43,0	880,8
27/2/15 18:00	27/2/15 21:00	28/2/15 1:00	8	1,7	10,4	1,6	2,9	10,4	2,0	30,5	214,9
5/3/15 7:00	5/3/15 12:00	6/3/15 7:00	25	2,3	11,4	1,8	3,7	10,9	3,0	58,8	905,6
18/3/15 18:00	20/3/15 17:00	22/3/15 10:00	89	4,0	10,4	2,3	6,3	9,0	3,0	167,1	5075,1
25/3/15 7:00	25/3/15 9:00	25/3/15 20:00	14	2,4	9,9	2,0	3,8	10,5	3,0	60,9	590,2
2/11/15 3:00	2/11/15 14:00	3/11/15 10:00	32	3,0		2,1	5,8		0,0	55,9	
26/11/15 10:00	27/11/15 0:00	27/11/15 5:00	20	2,1	11,1	1,8	3,2	10,7	1,0	47,6	695,8
15/2/16 19:00	16/2/16 0:00	16/2/16 11:00	17	2,2	11,3	2,0	3,4	11,0	0,0	56,0	731,2
20/4/16 13:00	20/4/16 17:00	20/4/16 19:00	7	1,7	7,9	1,6	2,7	7,9	0,0	22,4	136,4
9/5/16 0:00	9/5/16 10:00	10/5/16 10:00	35	2,1	8,0	1,7	3,3	8,1	1,0	36,8	843,4
14/11/16 23:00	17/11/16 4:00	17/11/16 6:00	56	1,7	8,6	1,5	2,8	7,2	0,0	24,9	923,6
16/12/16 21:00	19/12/16 6:00	21/12/16 23:00	123	3,4	9,0	2,1	5,9	9,0	1,0	105,4	4824,2
11/1/17 3:00	11/1/17 6:00	11/1/17 12:00	10	2,0	10,0	1,8	3,1	9,4	1,0	39,5	295,3
16/1/17 22:00	21/1/17 11:00	23/1/17 0:00	147	3,9	10,4	2,1	6,5	9,2	2,0	173,7	6772,4
8/2/17 19:00	9/2/17 2:00	9/2/17 3:00	9	1,9	10,5	1,7	2,9	10,3	2,0	35,9	272,8
12/2/17 21:00	13/2/17 11:00	14/2/17 2:00	30	2,1	8,9	1,7	3,1	8,5	3,0	39,0	709,1
13/11/17 6:00	14/11/17 0:00	14/11/17 16:00	35	2,5	11,6	2,0	3,9	11,1	0,0	74,0	1644,2
3/12/17 0:00	3/12/17 5:00	3/12/17 6:00	7	1,7	10,7	1,6	2,8	10,8	1,0	29,9	194,0
20/3/18 22:00	21/3/18 4:00	22/3/18 5:00	32	2,0	11,2	1,7	3,3	10,7	0,0	44,0	977,9
14/10/18 14:00	14/10/18 22:00	15/10/18 7:00	18	2,2	6,8	1,8	3,4	7,2	0,0	37,2	445,6
18/11/18 16:00	19/11/18 15:00	19/11/18 19:00	28	2,3	7,1	1,7	3,8	6,9	1,0	37,7	601,7
9/1/19 20:00	9/1/19 22:00	10/1/19 7:00	12	2,3	11,3	1,9	3,9	11,2	0,0	57,3	502,3
21/1/19 2:00	21/1/19 7:00	21/1/19 7:00	6	1,7	7,2	1,6	2,6	6,7	1,0	20,4	103,9
24/1/19 6:00	24/1/19 17:00	25/1/19 12:00	31	2,0	10,6	1,7	2,9	10,7	2,0	40,9	963,8
4/2/19 1:00	4/2/19 5:00	4/2/19 12:00	12	1,8	11,1	1,7	2,9	11,1	3,0	34,4	368,7
18/4/19 5:00	20/4/19 7:00	23/4/19 5:00	121	3,4	10,0	2,5	5,0	9,7	0,0	116,5	7635,3
11/11/19 2:00	11/11/19 8:00	12/11/19 6:00	29	2,2	11,3	1,4	3,7	10,2	0,0	52,6	675,1
3/12/19 22:00	4/12/19 4:00	4/12/19 23:00	26	3,1	8,4	2,2	5,0	8,4	1,0	81,4	1080,8
19/1/20 19:00	21/1/20 10:00	23/1/20 17:00	95	5,5	11,6	2,9	10,6	9,9	0,0	360,5	9014,5
4/2/20 21:00	5/2/20 3:00	5/2/20 6:00	10	1,9	10,4	1,7	3,0	10,4	1,0	36,1	305,4
16/3/20 9:00	17/3/20 17:00	18/3/20 7:00	47	2,3	9,0	1,9	3,7	8,4	1,0	45,8	1474,4
24/3/20 5:00	24/3/20 13:00	25/3/20 12:00	32	2,3	7,7	1,9	3,9	7,5	1,0	40,3	887,6
31/3/20 7:00	31/3/20 23:00	2/4/20 1:00	43	1,9	6,2	1,5	3,1	6,6	2,0	22,9	611,3
15/4/20 22:00	16/4/20 4:00	16/4/20 14:00	17	2,0	8,9	1,7	3,2	8,1	3,0	35,6	411,7
8/5/20 9:00	8/5/20 12:00	9/5/20 11:00	27	1,9	7,5	1,7	3,1	7,8	3,0	29,9	592,6
20/10/20 23:00	21/10/20 1:00	21/10/20 11:00	13	1,8	7,0	1,6	2,8	7,5	0,0	25,0	264,0
5/11/20 20:00	6/11/20 20:00	7/11/20 18:00	47	2,1	7,2	1,7	3,3	7,2	1,0	30,4	1037,2
20/11/20 3:00	20/11/20 11:00	21/11/20 0:00	22	2,1	11,0	1,8	3,3	10,4	2,0	48,0	727,9
28/11/20 8:00	28/11/20 12:00	28/11/20 21:00	14	2,0	8,7	1,7	3,2	8,6	3,0	33,0	346,0
7/1/21 15:00	7/1/21 18:00	9/1/21 13:00	47	1,8	6,6	1,4	2,9	6,4	1,0	22,2	578,4
21/2/21 7:00	21/2/21 19:00	22/2/21 17:00	35	2,6	7,7	1,9	4,1	8,2	1,0	52,0	1040,5
1/3/21 23:00	2/3/21 11:00	3/3/21 18:00	44	1,9	8,1	1,6	3,1	7,9	1,0	28,0	944,9
20/3/21 12:00	20/3/21 14:00	20/3/21 22:00	11	2,0	5,7	1,7	3,3	8,4	2,0	31,7	262,4
9/4/21 9:00	9/4/21 19:00	10/4/21 6:00	22	2,0	8,3	1,7	3,2	8,0	2,0	31,7	523,4
1/9/21 21:00	1/9/21 23:00	2/9/21 11:00	15	1,9	6,3	1,6	2,6	6,5	0,0	21,8	250,0
24/9/21 0:00	24/9/21 3:00	24/9/21 18:00	19	2,1	7,3	1,7	3,2	7,9	1,0	31,1	457,2
5/11/21 23:00	6/11/21 8:00	10/11/21 14:00	112	2,9	10,4	1,8	4,5	9,8	0,0	86,0	3726,1
15/11/21 19:00	15/11/21 22:00	16/11/21 9:00	15	1,8	10,1	1,5	3,0	9,8	1,0	30,8	343,3
1/2/22 3:00	1/2/22 6:00	1/2/22 14:00	12	1,8	11,2	1,6	2,7	11,0	0,0	37,5	352,3
14/3/22 9:00	15/3/22 8:00	30/3/22 4:00	380	3,0	10,4	2,0	4,8	8,7	0,0	96,2	13861,9
11/4/22 21:00	13/4/22 20:00	15/4/22 7:00	83	2,2	8,6	1,7	3,4	8,6	1,0	41,4	2072,8
5/5/22 2:00	5/5/22 7:00	5/5/22 10:00	9	1,7	7,2	1,6	2,8	7,4	2,0	22,0	174,8